Final Report
June 15, 2005
ONR Contract Number N000-14-01-1-1065
Direct Manufacture of Components with Local Control of Composition

Emanuel Sachs
Fred Fort Flowers and Daniel Fort Flowers Professor of Mechanical Engineering
Massachusetts Institute of Technology
Room 35-136
77 Massachusetts Avenue
Cambridge, MA 02139
Tel: 617.253.5381, Fax: 617.253.0209
email: sachs@mit.edu

Overview and Summary

One of the great potentials of Solid Freeform Fabrication (SFF) is the ability to create parts which have different composition in different locations. This capability stems from the fundamental additive nature of SFF technologies. Three Dimensional Printing in particular is extremely flexible in this regard as material composition can be controlled not only between layers but also within a layer by printing different materials into different locations in the layer. The purpose of this work was to explore the potential of 3D Printing to create two different classes of components with local control of composition; gradient index lenses (GRIN) and metallic components with local composition control. These two classes of application are complimentary in that the GRIN lenses were made of glasses and were fabricated from extremely fine powders handled in a slurry form while the metallic components were fabricated from larger powders that can be dry processed.

Pages 2-8 provide a summary of our work on GRIN lenses. Appendix A contains a paper which has appeared in *Advances in Photonic Materials and Devices* and Appendix B contains a paper on GRIN lenses which as been submitted to the *Journal of Non-Crystalline Solids*.

Pages 9-12 contain a description of the work done on printing of metallic components by Three Dimensional Printing. The focus of this work was on demonstrating the principal by creating a bimetallic structure and testing its response to temperature changes. This work is well documented in the Master's thesis of Ratchatee Techapiesancharoenkij entitled "Bimetallic Bars with Local Control of Composition by Three-Dimensional Printing" (http://libraries.mit.edu/help/mit-thesis.html).

Local Composition Control By 3DP Applied To Gradient Index Lenses

1. INTRODUCTION

The S-3DP™ technology is an agile, facile method of producing near-net shape advanced ceramic components. Parts are constructed in a layer-by-layer build sequence. Each powder bed layer is created by jetting a ceramic slurry onto a substrate. The as-cast layer is then dried and a binder, which cements the ceramic particles, is selectively deposited in the desired pattern. The excess powder is then removed to produce a three dimensional structure. The S-3DP™ process can be modified to fabricate functionally graded materials, such as GRIN lenses, by depositing different amounts of dopant instead of a binder into each layer. The S-3DP™ process for GRIN lenses is shown schematically in Figure 1. Production of GRIN materials by S-3DP™ offers several advantages over conventional processing methods, including reduced processing times (< 70 hours) yielding economical fabrication of large-scale components, improved compositional flexibility, and increased index profile dimensionality. The improved flexibility and compositional control offered by S-3DP™ results in a single component lens system with greater functionality. The lens stacking required to overcome optical aberrations of a photographic lens system can be eliminated by taking advantages of the additional degree of freedom offered by S-3DP™ GRIN lenses. This reduces the number of optical components required, yielding considerable weight savings.

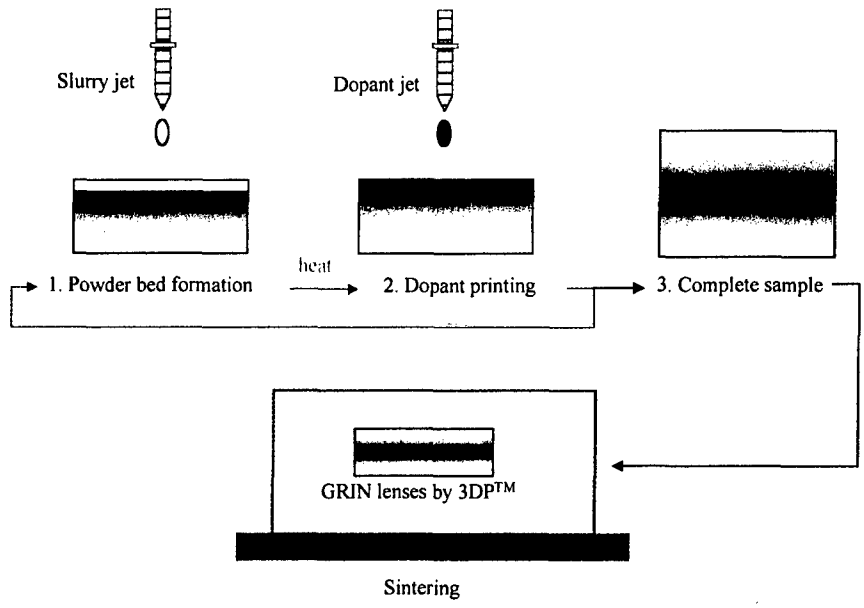

Figure 1. The schematic drawing of the S-3DP™ process for GRIN lenses.

2. EXPERIMENTAL PROCEDURE

2.1 Printing Designs and Conditions

Alumina-silica powder beds with vertical compositional variation were fabricated by S-3DP™. The thickness of each printed layer was 73 μm. The vertical dopant concentration profiles for the alumina-silica systems are shown in Figure 2. Each printed slurry layer and dopant layer was dried at 65 °C for 50 seconds.

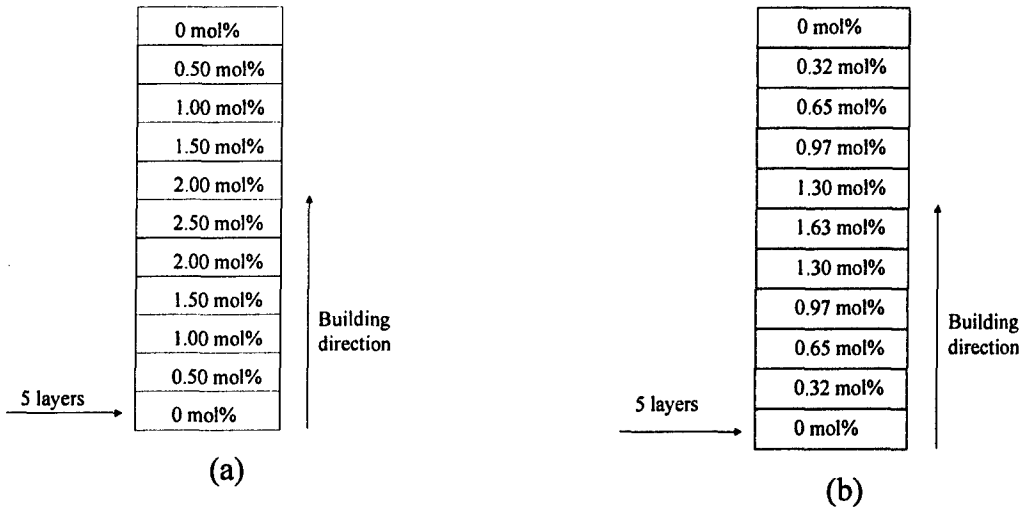

Figure 2. The concentration profiles of alumina in the GRIN lenses of (a) Design 2.5% max and (b) Design 1.63% max.

GRIN lenses with radial compositional variation were made by the 3DP™ machine from TDK. Drop-on-Demand (DoD) printing nozzles, which allow the dopant solution to be deposited in selective region drop by drop, were used to deposit aluminum nitrate solution with the drop size of 45 μm. The thickness of each slurry layer was 40 μm. The designed concentration profile is shown in Figure 3. Each printed slurry layer was dried at 100 °C for 50 seconds. Half of the total dopant drops for each layer were printed and dried in a microwave oven for 1 minute, then the rest of the dopant drops were printed and dried.

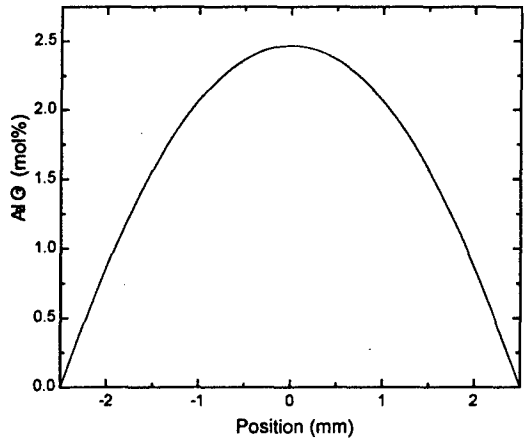

Figure 3. The concentration profile of the GRIN lens with radial index variation

2.2 Materials and Slurry Preparation

The amorphous silica powder (Mitsubishi Chemical Company) used in this research had a median particle size of 1.4 μm and a surface area of 2.666 m^2/g. Water-soluble aluminum nitrate nanohydrate ($Al(NO_3)_3*9H_2O$, Alfa Aesar) was used as dopant sources. Vertical index variation GRIN lenses were fabricated from a 30 vol% silica slurry, while a 22.5 vol% slurry was used to fabricate radial index variation GRIN lenses. Both slurries were ball-milled with glass media for 20 hours before printing. The chemical compositions of the slurries are shown in Table I. Boric Acid was added to lower the sintering temperature.

Table I. The chemical compositions of the silica slurries.

Silica Powder (vol%)	Deionized Water (vol%)	Methanol (vol%)	2-Propanol (vol%)	Poly (ethylene glycol) (MW:400)	TMAH* (M)	NH4OH (M)	H3BO3 (wt%)
30	35	35	0	3 wt% based on silica	0	0.20	1 wt% based on silica
22.5	38.75	0	38.75	0	0.063	0	1 wt% based on silica

*tetramethylammonium hydroxide

2.3 Heat Treatment and Sintering

The alumina-silica powder beds were heated at a higher temperature of 900°C for 4 hours to remove the hydroxyl groups introduced by the aluminum nitrate solution as well as the organic additives. Sintering was performed in a vacuum furnace (Centoor, MRF, pressure ~ $5x10^{-6}$ torr) at various temperatures, holding times, and cooling rates. It was found that un-doped silica powder beds were sintered into optical transparency at 1500°C for 30 minutes.

2.4 Sample Characterization

X-ray Diffraction (XRD) was used to detect crystallization of the doped powder bed after heat treatment. Chemical composition of the doped powder beds were measured by Electron Probe Microanalysis (EPMA) with JOEL Superprobe 733.

3. RESULT

3.1 Sintering of Alumina-Silica GRIN Lenses

The mixture of alumina and silica tends to form mullite ($3Al_2O_3+2SiO_2$) at temperature higher than 950 °C[1]. The formation of mullite can be minimized by increasing the cooling rate and using the alumina concentration lower than 5 mol%[1]. The maximum alumina concentration in this study was 2.50 mol% (Figure 5). XRD detected no crystallization in the alumina-silica powder beds that were treated at 900 °C for 4 hours, as shown in Figure 4. Several sintering conditions were tested. Optical transparency was achieved for the powder bed of a maximum alumina concentration with 1.63 mol% by sintering at 1650 °C for 30 minutes and cooling at the maximum rate (~500 °C/minute from the sintering temperature) allowed by the furnace. An additional dehydration process at 1000 °C for 24 hours in either the vacuum furnace or a 3% Cl_2 atmosphere for powder beds with a maximum alumina concentration of 2.50 mol% was required to completely remove the residual hydroxyl groups that form bubbles during sintering.

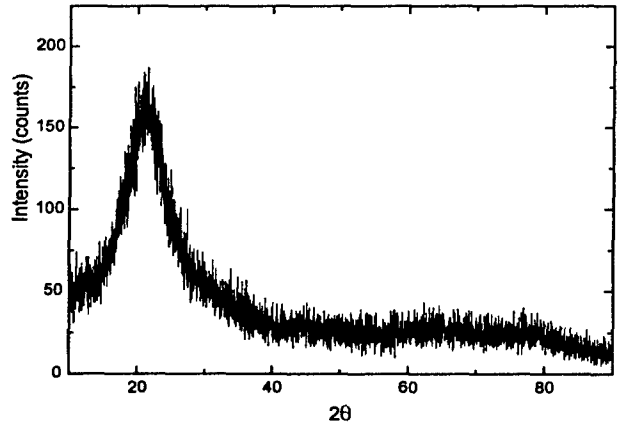

Figure 4. The XRD result of the alumina-silica powder bed treated at 900 °C for 4 hours.

3.2 GRIN Lenses with Vertical Index Variation

The magnifying effects of the sintered silica-alumina powder beds with vertical compositional variation are shown in Figure 5. The MIT markers under the sintered GRIN lenses are magnified in the vertical direction, as expected from the dopant concentration profile shown in Figure 2. The object and image sizes in the vertical direction were measured, allowing the effective focal length (f_{eff}) to be determined by the following equation[2]:

$$\frac{1}{f_{eff}} = \frac{1}{S_1} - \frac{H_1}{H_2 * S_1} \qquad (1)$$

where H_1 is the object size, H_2 is the image size, and S_1 is the distance between the lens and the object. The theoretical focal length (f_{th}) of a GRIN slab with a parabolic index of refraction profile is given by the following equation[3]:

$$f_{th} = \frac{1}{\left(\frac{n_{max}^2 - n_{min}^2}{0.25w^2}\right)^{1/2} \sin\left(\frac{d}{0.5w}\left(1 - \frac{n_{min}^2}{n_{max}^2}\right)^{1/2}\right)} \qquad (2)$$

where w is the width of the GRIN slab, d is the thickness of the GRIN slab, n_{min} is the minimum index of refraction, and n_{max} is the maximum index of refraction. No direct measurement of index of refraction has been made. The index of refraction, n, of fused silicate containing alumina has been found to vary linearly relationship with the alumina content, M, as described by Equation 3: [4]

$$n = 1.4580 + 0.00192M \qquad (3)$$

where M is the alumina concentration in mol%. The alumina concentration profiles of the Design 1.63% max and Design 2.5% max samples are shown in Figure 6. The profiles are fitted with parabolic curves. The actual maximum alumina concentrations of the Design 1.63% max and Design 2.5% max samples were found to be 1.04 mol% and 1.35 mol% and the maximum indices of refraction (n_{max}) of the samples were calculated to be 1.46 and 1.4606 from Equation (3). The theoretical focal lengths of the sintered powder beds, assuming a parabolic index profile, were then calculated and compared with the effective focal lengths, as shown in Table II. The effective focal length is very close to the theoretical values for the Design 1.63% max sample. The difference between the effective and theoretical values of the Design 2.5% max and Design 2.5% max(1) samples is due to the fact that the index profiles are not ideally parabolic. The actual concentrations are also lower than the designed values.

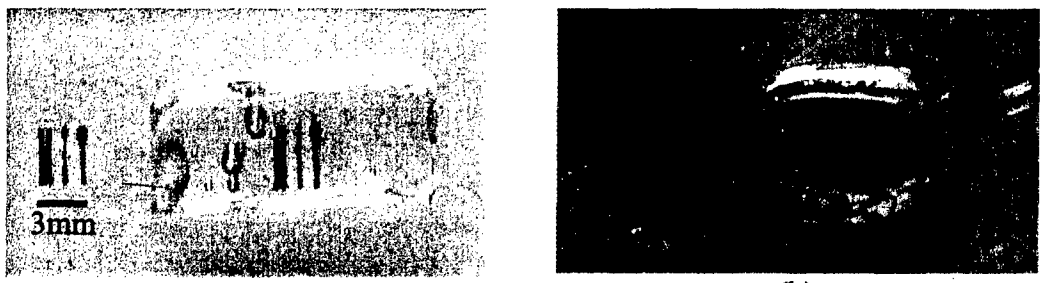

(a) (b)

Figure 5. The vertical enlargement with the alumina-doped GRIN lenses above an MIT marker. (a)Maximum alumina concentration: 1.63 mol%, (b)Maximum alummina concentration: 2.50 mol%

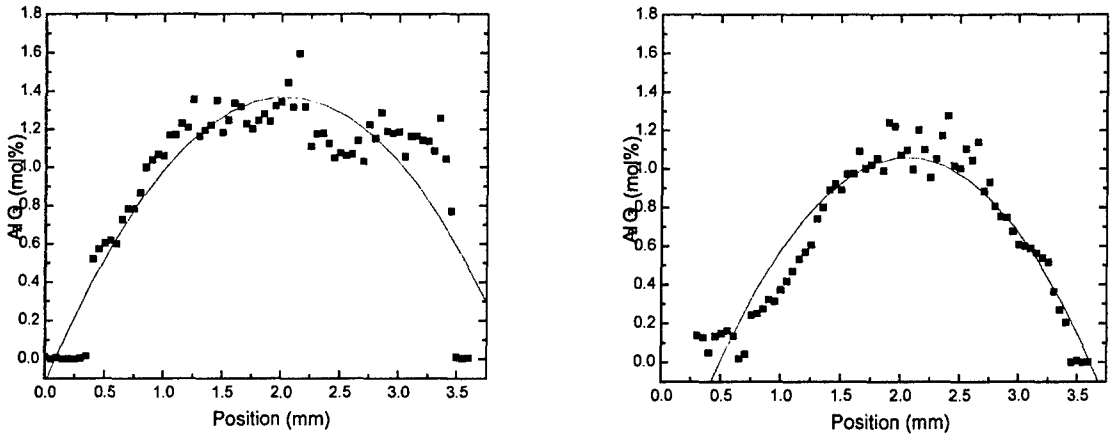

(a) (b)

Figure 6. The dopant distribution of the GRIN lenses of (a) Design 2.5% max(1) and (b) Design 1.63% max

Table II. The effective (f_{eff}) and theoretical (f_{th}) focal lengths of different GRIN lenses

	d (cm)	w (cm)	f_{eff}(cm)	f_{th} (cm)
Design 1.63% max	0.55	0.30	10	10.3
Design 2.5% max	0.70	0.30	4.68	6.27
Design 2.5% max (1)	0.60	0.30	6.10	7.28

3.3 GRIN Lenses with Radial Index Variation

The magnifying effects of the sintered powder beds with radial compositional variation are shown in Figure 7. The letter under the sintered sample is magnified horizontally and vertically, as expected from the dopant concentration profile shown in Figure 3. The effective focal lengths in x-direction and y-direction are calculated to be 33.75 cm and 29.06 cm. The alumina concentration profile of the sample is shown in Figure 8. Considering the alumina concentration in the center region of both profiles, the maximum alumina concentrations in x-direction and y-direction were both found to have a value about 1.57 mol%. The theoretical focal length was then calculated to be 30.5 cm from Equation 2. It is noted that actual maximum alumina concentration is lower than the designed values, as in the case of the vertical index variation GRIN lenses.

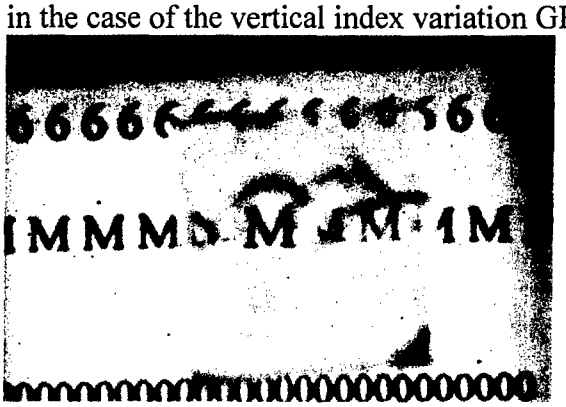

Figure 7. The enlargement with the alumina-doped GRIN lenses.

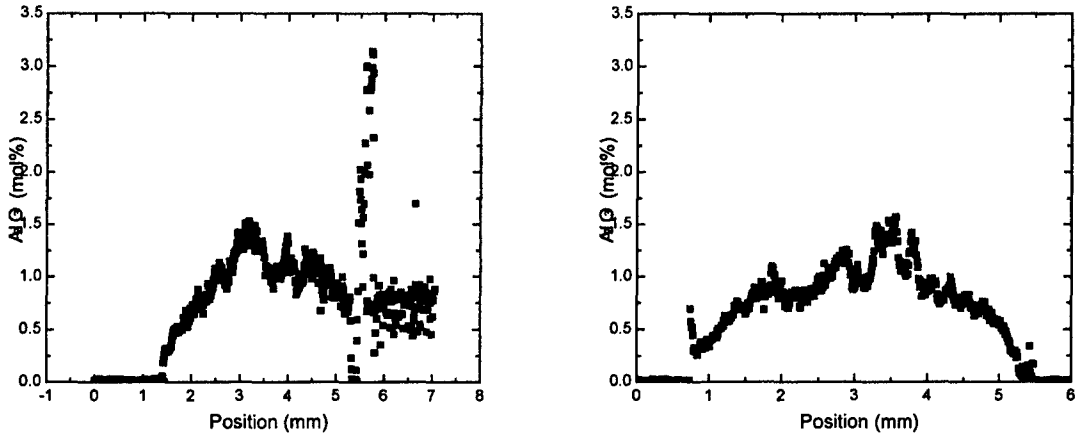

(a) (b)

Figure 8. The dopant distributions of the GRIN with radial index variation in (a) x-direction and (b) y-direction.

4. SUMMARY

The alumina-silica systems have been studied for the fabrication of GRIN lenses by S-3DP™. Optically transparent alumina-silica GRIN lenses were obtained by sintering at 1650 °C for 30 minutes. Three different GRIN lenses with vertical index variation (Design 1.63% max, Design 2.5% max and Design 2.5% max(1)) with effective focal lengths of 10, 4.68, and 6.10 cm, respectively, have been successfully fabricated. DoD printheads were used to fabricate GRIN lenses with radial index variation. The effective focal lengths in the x-direction and y-direction were measured to be 33.75 cm and 29.06 cm, respectively.

5. REFERENCES

[1] J.F. MacDowell and G. H. Beall, ""Immiscibility and Crystallization in Al_2O_3-SiO_2 Glasses," *J. Am. Ceram. Soc.*, **52** [1] 17-25 (1969).

[2] E. Hecht, "Optics," 4th edition, Addison-Wesley, 2002.

[3] B. E. A. Saleh and M. C. Teich, "Fundamentals of Photonics," John Wiley & Sons Inc., New York, 1991.

[4] K. Nassau, J. W. Shiever, and J. T. Krause, "Preparation and Properties of Fused Silica Containing Alumina," *J. Am. Ceram. Soc.*, **58** [9-10] 461 (1975).

Bimetallic Bars with Local Control of Composition by Three-Dimensional Printing

The fabrication of metallic components with LCC by 3DP is the subject of this work. Specifically, LCC was studied and demonstrated by fabricating bimetallic bars consisting of two layers of Fe-Ni alloys with different composition and, hence, different thermal expansion properties. When the bars are subject to a temperature change, they bend due to the different coefficients of thermal expansion (CTE).

Generally, a bimetallic strip consists of a low CTE alloy bonded to a high CTE alloy. As a result, to make a bimetallic strip with LCC, a material system whose CTE is sensitive to its composition is desired. Such behavior is found in the Fe-Ni alloy system. Figure 1 shows the thermal expansion coefficient curve as a function of composition in an Fe-Ni system. The Fe-Ni alloy with 35 at% Ni has a very small thermal expansion coefficient of less than $1.2 \times 10^{-6}\ C^{-1}$ at a room temperature.

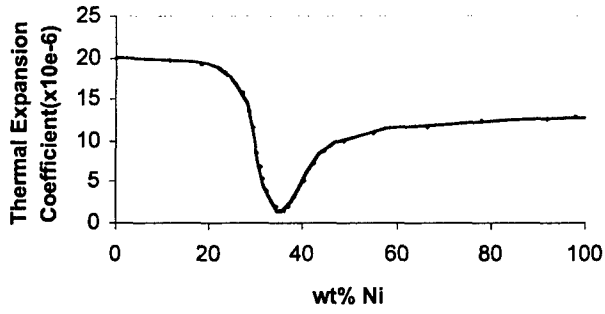

Figure 1 Thermal Expansion Coefficients as a function of Ni contents in an Fe-Ni alloy.

A procedure of the fabrication of an LCC bimetallic bar is schematically shown in Figure 2. First, a powder bed of Fe-30wt%Ni powders was spread. Then, an Fe_2O_3 slurry was printed onto the powder so that the final Fe content increased. By successive printing of such layers, an iron-enriched volume of arbitrary thickness was produced. Then, by repeating the process with a NiO slurry, a nickel-enriched volume was printed resulting in a bimetallic part with regions locally enriched in iron adjacent to regions enriched in nickel. The printed bars before firing and retrieval are shown in Figure 3. After completion of printing, the printed bar was heated at 400 °C so that the oxide particles were reduced to Fe or Ni particles. The small Fe and Ni particles sinter faster and at a lower temperature than the larger base Fe-30Ni powders. These small powders sinter and form interparticle bonds that impart strength the printed part. As a result, the printed bars were successfully retrieved from unbound powders (Figure 4a). Then, the bars were fired more at 800 °C for 1 hour for more strengthening. Finally, the bars were annealed at 1400 °C for 2 hours for sintering and local homogenization. The final composition of the base powders were changed accordingly (Figure 5a). In the layers on

which an Fe_2O_3 slurry was printed, the Fe composition of the layers increased on average to 72wt%. Similarly, the Ni composition of the Ni-enriched layers of the bars increased on average to 33wt%.

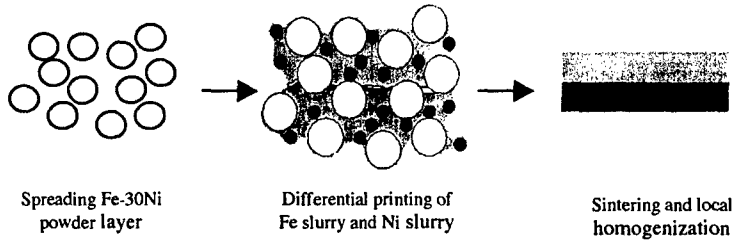

Figure 2 Schematic illustration of the fabrication of a Fe-Ni bimetallic bar with LCC.

Figure 3 The printed bars before firing and retrieval processes.

Figure 4 The retrieved bars (A) after firing at 400 °C for 1 hour and (B) after firing more at 800 °C for 1 hour.

The densification and local homogenization resulting from reduction and sintering treatments were not satisfactory. The major problem was presumably caused by the oxide residues. The presence of the oxide powders was evident from the microprobe measurement. The oxide residues caused the local compositions to be inhomogeneous.

As a result, the compositional profile (Figure 5a) showed considerable scatter. Moreover, the residues impeded the sintering rate of the bars; the sintering densities of the bars were as small as 78% of the theoretical density as evident from the microstructure images (Figure 5b) showing a large volume fraction of pores inside the bars.

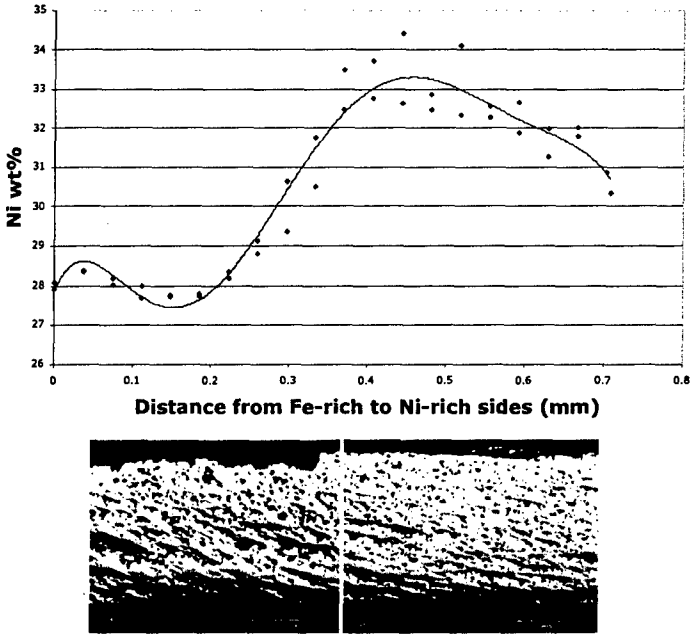

Figure 5 (A) the compositional profile of the bimetalling bar (top) and (B) microstructures of the bimettalic bars (bottom).

The resulting bimetallic bars did exhibit bending deflection on uniform heating (Figure 6). However, the bending deflections were much smaller than expected. The maximum deflection (*a*) of the bar, with a dimension of 63mmx45mmx0.68mm, is 0.6 mm at 400 °C. Evidently, the compositional profiles of the bars critically influence their thermal bending properties. The scatter in the compositional profiles resulted in local variations of CTE in the bars, which degraded the thermal bending properties.

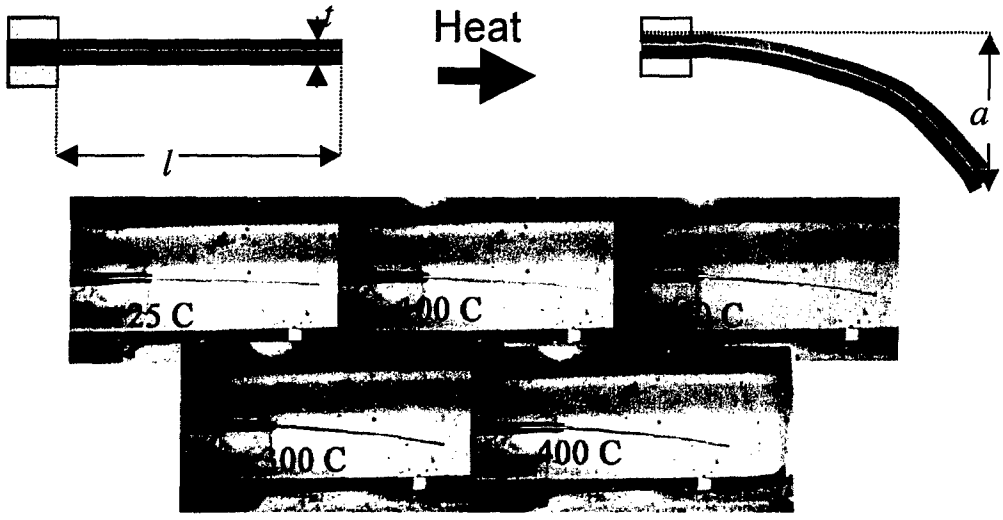

Figure 6 The picture of an LCC bimetal bar while bending as heated

APPENDIX A

GRADIENT-INDEX (GRIN) LENSES AND OTHER OPTICAL ELEMENTS BY SLURRY-BASED THREE DIMENSIONAL PRINTING

Hong-Ren Wang and Michael J. Cima
Department of Materials Science and Engineering
Massachusetts Institute of Technology
77 Massachusetts Avenue
Cambridge, MA 02139

Brian D. Kernan and Emanuel M. Sachs
Department of Mechanical Engineering
Massachusetts Institute of Technology
77 Massachusetts Avenue
Cambridge, MA 02139

ABSTRACT

The slurry-based three-dimensional printing (S-3DP™) process has been used to fabricate complex ceramic structure materials by printing organic binders in selective positions of each printing layer. S-3DP™ has the advantages of short processing time and ability to control fine structures in bulk materials. This process has been modified to fabricate functionally graded materials by depositing different concentrations of dopant into selective positions. Functionally graded optical elements can be made when index-changing materials are printed. S-3DP™ provides the control of index variation in three dimensions inside bulk optical materials. Alumina-doped silica was chosen to demonstrate the fabrication of functionally graded optical elements. Aluminum nitrate, which decomposes into alumina during heat treatment, was dissolved in deionized water and printed into the silica powder bed with a maximum concentration of 2.5 mol%. The alumina-doped powder bed was dehydrated at 1000 °C for 24 hours and sintered at 1650 °C for 30 minutes in a vacuum furnace ($5x10^{-6}$ torr). Alumina-doped silica GRIN lenses with axial and radial index variations have been successfully fabricated using S-3DP™. The distribution of alumina after sintering was measured by Electron Probe Microanalysis (EPMA) and compared with the design profile. The resulting optical effect was examined by measuring the effective focal length of the GRIN lens and compared with the theoretical value. Other optical elements, such as volume phase grating elements, will also be discussed.

INTRODUCTION

Conventional glass-based GRIN lenses, as shown in Fig. 1, have been fabricated by various methods, including molecular stuffing[1], ion exchange[2-7] and sol-gel[8,9] techniques, which rely on stuffing of base glass compositions with index altering cations. The diffusion-controlled nature of these processes results in long processing times (typically > 100 hours), thereby limiting feasible component sizes to less than 13 mm. A comparison of the lens diameter and the index gradient difference (Δn) of radial GRIN rods prepared by various methods is provided in Fig. 1[8]. The maximum index gradient difference currently produced, i.e., $\Delta n < 0.2$, is limited not only by the base glass composition, but the dopant concentration profiles achievable by these methods. Commercially available SELFOC® lenses, for example, prepared by ion exchange exhibit a maximum Δn value of 0.124 for components ranging in size from 1.0 to 4.5 mm[10]. GRIN materials fabricated by ion exchange techniques are also not suitable for high temperature applications because the migration of alkali ions results in the distortion of the index profile[8]. Alternative materials systems or fabrication methods for large-scale GRIN components with desired optical characteristics and good environmental and thermal stability are needed.

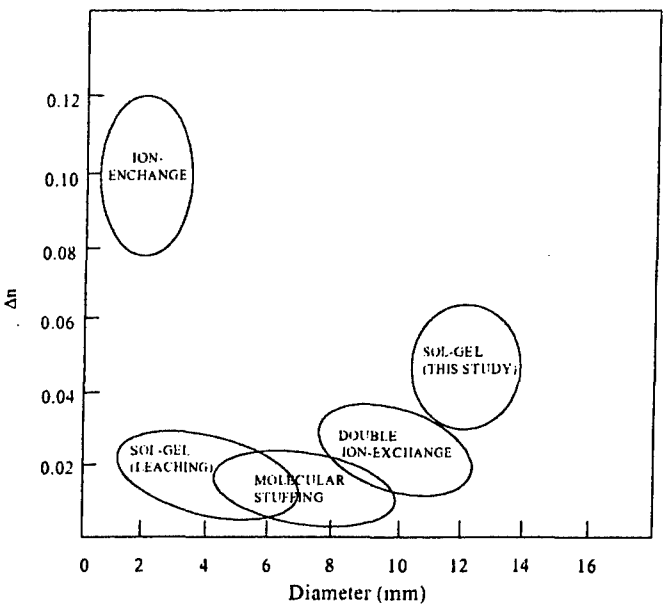

Fig. 1. Comparison of the lens diameter and Δn of radial GRIN rods prepared by various methods.[8]

Microlens arrays have been used for the interconnection between optical fibers. The optical signal is refocused when passing through individual microlens. Commercially available microlens arrays are typically made of polymer-based or glass-based materials, such as UV curable polymer and borosilicate. The focusing powder of these microlens arrays results from the curvature of individual microlens except the SELFOC® microlens array that consists of an array of GRIN lenses. The focusing powder and the lens-to-lens distance determine the performance of a microlens array. Volume phase gratings are used as filters in various applications such as Raman spectroscopy[11] and confocal microscope[12]. It is known that volume phase gratings provide higher light transmission than the traditional amplitude gratings. Volume phase gratings are typically made by shining diffraction pattern generated from two laser sources onto photosensitive materials such as dichromated gelatin and iron-doped lithium niobate. The size and depth of the grating are generally limited by the powder of laser and the photosensitive materials.

The S-3DP™ technology[13-15] is an agile, facile method of producing near-net shape advanced ceramic components. Parts are constructed in a layer-by-layer build sequence. Each powder bed layer is created by jetting a ceramic slurry onto a substrate. The as-cast layer is then dried and a binder, which cements the ceramic particles, is selectively deposited in the desired pattern. The excess powder is then removed to produce a three dimensional structure. The S-3DP™ process can be modified to fabricate functionally graded materials, such as GRIN lenses, by depositing different amounts of dopant instead of a binder into each layer. The S-3DP™ processes for vertical and radial GRIN lenses are shown schematically in Fig. 2(a) and Fig. 2(b), respectively. Production of GRIN materials by S-3DP™ offers several advantages over conventional processing methods, including reduced processing times (< 70 hours) yielding economical fabrication of large-scale components, improved compositional flexibility, and increased index profile dimensionality. The improved flexibility and compositional control offered by S-3DP™

results in a single component lens system with greater functionality. The lens stacking required to overcome optical aberrations of a photographic lens system can be eliminated by taking advantages of the additional degree of freedom offered by S-3DP™ GRIN lenses. This research attempts to demonstrate the concept of utilizing S-3DP™ to the fabrication of larger scale GRIN lenses and other optical elements, including micro lens arrays and optical volume phase gratings. Several silica-based material systems have been considered and tested. The alumina-doped silica glass was chosen as the material system.

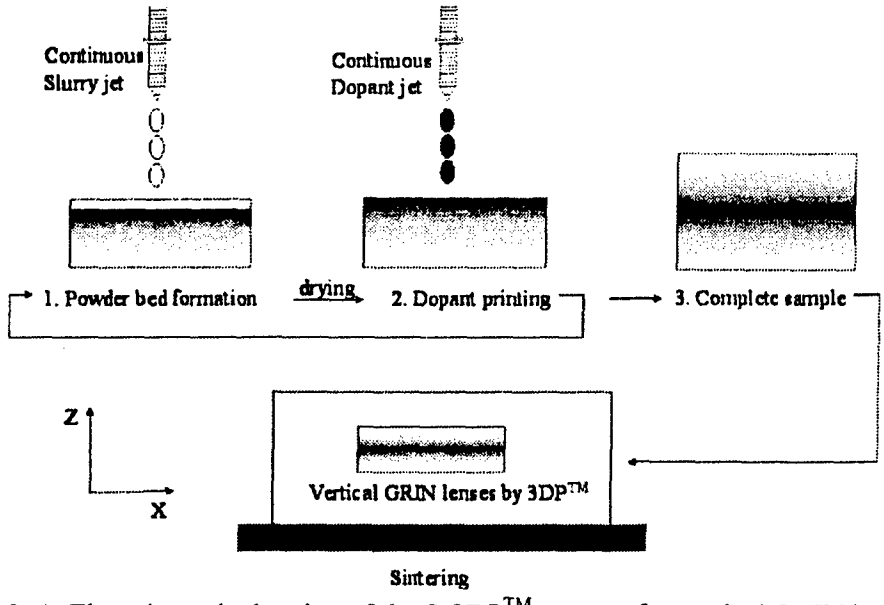

Fig. 2(a). The schematic drawing of the S-3DP™ process for vertical GRIN lenses.

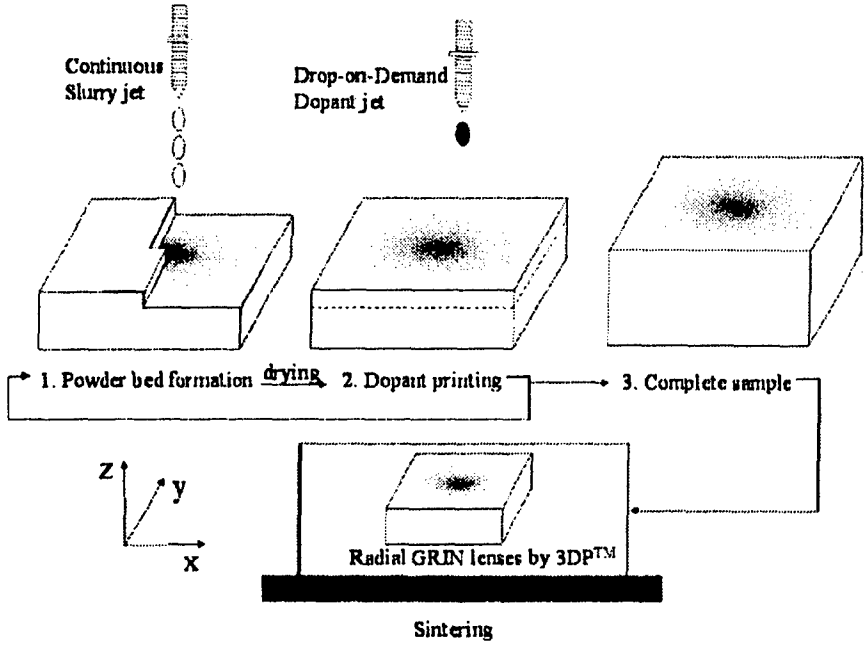

Fig. 2(b). The schematic drawing of the S-3DP™ process for radial GRIN lenses.

EXPERIMENTS

The amorphous silica powder (Mitsubishi Chemical Company) used in this research had a median particle size of 1.4 μm and a surface area of 2.666 m^2/g. Aluminum nitrate nanohydrate ($Al(NO_3)_3*9H_2O$, Alfa Aesar) was used as the dopant source. Vertical index variation GRIN lenses were fabricated from a 30 vol% silica slurry, while a 22.5 vol% slurry was used to fabricate the radial index variation GRIN lens. Both slurries were ball-milled with glass media for 20 hours before printing. The chemical compositions of the slurries are shown in Table I. Boric Acid was added to lower the sintering temperature.

Table I. The chemical compositions of the silica slurries.

Silica Powder (vol%)	Deionized Water (vol%)	Methanol (vol%)	2-Propanol (vol%)	Poly (ethylene glycol) (MW:400)	TMAH* (M)	NH4OH (M)	H_3BO_3 (wt%)
30	35	35	0	3 wt% based on silica	0	0.20	1 wt% based on silica
22.5	38.75	0	38.75	0	0.063	0	1 wt% based on silica

*tetramethylammonium hydroxide

Aluminum nitrate-doped silica powder beds with vertical compositional variation were fabricated by S-3DP™ using a continuous dopant jet. The vertical compositional variation was achieved by printing different concentrations of aluminum nitrate solution while keeping the flow rate of the continuous dopant jet unchanged. The thickness of each printed layer was 73 μm. Two vertical concentration profiles with maximum concentration in the center were printed to create two vertical GRIN lenses with different optical effects, shown in Fig. 3. Each printed slurry layer and dopant layer was dried at 65 ^0C for 50 seconds and 55 layers were printed. Aluminum nitrate-doped silica powder beds with radial compositional variation were made with a 3DP™ machine equipped with Drop-on-Demand (DoD) printing nozzles, which allow the dopant solution to be deposited in selective region drop by drop. The drop size of the aluminum nitrate solution was 45 μm. The thickness of each dried slurry layer was 40 μm. The designed concentration profile is shown in Fig. 4. Each printed slurry layer was dried at 100 ^0C for 50 seconds while each printed dopant layer was dried in a microwave oven for 1 minute. Microlens arrays were made by printing individual dopant drops into a silica powder bed with a drop-to-drop distance of 120 μm. One layer of the array pattern was printed. Two line patterns of the volume phase grating samples were also printed using DoD printing nozzles with the printing line spacing of 120 μm and 160 μm, respectively.

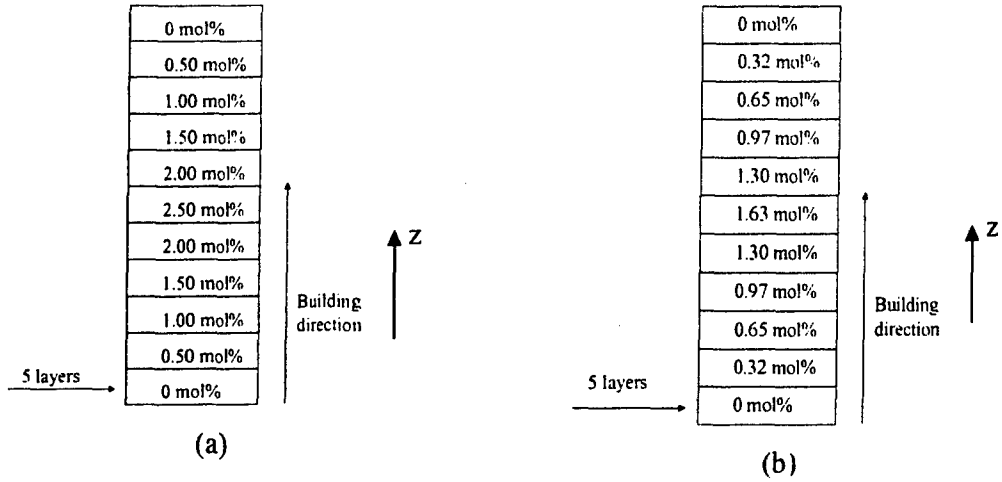

Fig. 3. The concentration profiles of alumina in the GRIN lenses of (a) Design 2.5% max and (b) Design 1.63% max.

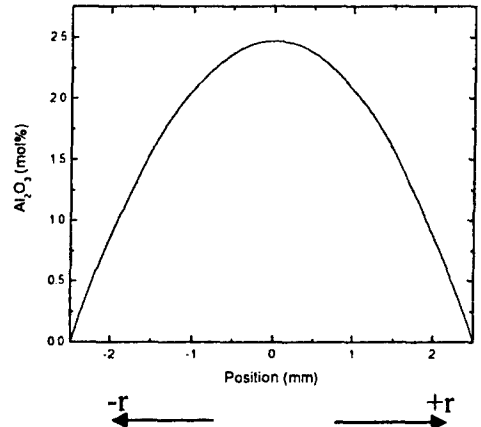

Fig. 4. The concentration profile of the GRIN lens with radial index variation

The aluminum nitrate-doped silica powder beds were heated at a temperature of 900°C for 4 hours in air to remove the hydroxyl groups introduced by the aluminum nitrate solution as well as the organic additives. Sintering was performed in a vacuum furnace (Centoor, MRF, pressure ~ $5x10^{-6}$ torr) at various temperatures, holding times, and cooling rates. It was found that un-doped silica powder beds were sintered into optical transparency at 1500°C for 30 minutes, as shown in Fig. 5. An additional dehydration process at 1000 °C for 24 hours in the vacuum furnace for powder beds with a maximum alumina concentration of 2.50 mol% or higher was required to completely remove the residual hydroxyl groups that form bubbles during sintering.

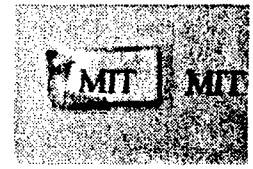

Fig. 5. The transparent un-doped silica powder bed sintered at 1500 °C for 30 minutes.

X-ray Diffraction (XRD) was used to detect crystallization of the doped powder bed after heat treatment. The sintered powder beds were polished and observed under an optical microscope. Chemical compositions of the doped powder beds were measured by electron probe microanalysis (EPMA, JOEL Superprobe 733).

RESULTS

The mixture of alumina and silica tends to form mullite ($3Al_2O_3+2SiO_2$) at temperature higher than 950 °C[14]. The formation of mullite can be minimized by increasing the cooling rate and using the alumina concentration lower than 5 mol%[16]. The maximum alumina concentration in this study was 2.50 mol% (Fig. 4). XRD result shows no crystallization in the alumina-silica powder beds that were treated at 900 °C for 4 hours. Several sintering conditions were tested. Optical transparency was achieved for the alumina-doped powder beds by sintering at 1650 °C for 30 minutes and cooling at the maximum rate (~500 °C/minute from the sintering temperature) allowed by the furnace.

The magnifying effects of the sintered powder beds with vertical compositional variation are shown in Fig. 6. The MIT markers under the sintered powder beds are magnified in the vertical direction, as expected from the dopant concentration profile shown in Fig. 3. The object and image sizes in the vertical direction were measured, allowing the effective focal length (f_{eff}) to be determined by the following equation[17]:

$$\frac{1}{f_{\text{eff}}} = \frac{1}{S_1} - \frac{H_1}{H_2 * S_1} \qquad (1)$$

where H_1 is the object size, H_2 is the image size, and S_1 is the distance between the lens and the object. The effective focal lengths of the powder beds with vertical compositional variation were calculated to be 10 cm and 6.1 cm for Design 1.63% max and Design 2.50 max, respectively. The magnifying effect of the sintered powder bed with radial compositional variation is shown in Fig. 7. The effective focal lengths were also calculated to be 63.75 cm in x-direction and 52.50 cm in y-direction using the same method.

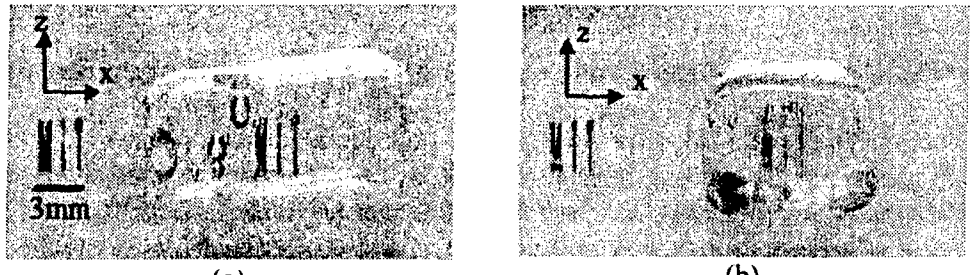

(a) (b)

Fig. 6. The vertical enlargement with the alumina-doped GRIN lenses above an MIT marker. (a)Maximum alumina concentration: 1.63 mol%, (b)Maximum alummina concentration: 2.50 mol%

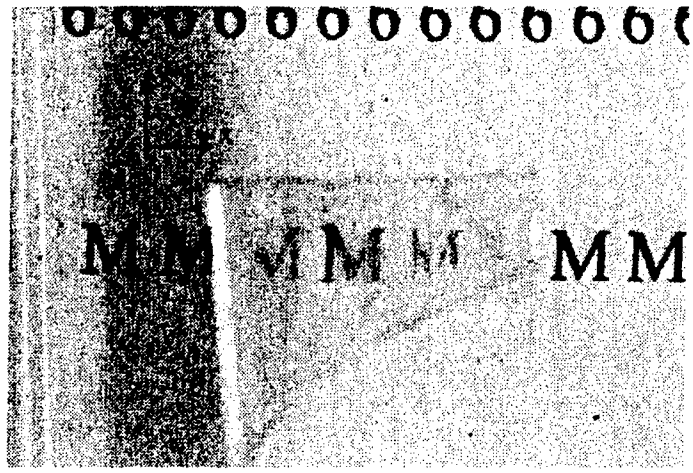

Fig. 7. The enlargement with the radial alumina-doped GRIN lenses.

The chemical composition profiles of the sintered powder beds with vertical compositional variation measured by EPMA are shown in Fig. 8 while the chemical composition profiles in x-direction and y-direction of the sintered powder bed with radial compositional variation are shown in Fig. 9. The EPMA mapping result of the sintered microlens array is shown in Fig. 10. The average microlens size can be measured from Fig. 10 to be about 77 μm while the dot-to-dot distance in both x-direction and y-direction is about 90 μm. Fig. 11 shows the EPMA results of the sintered volume phase gratings. The average line spacing after sintering can be measured from Fig. 11 to be 135 μm and 104 μm, respectively.

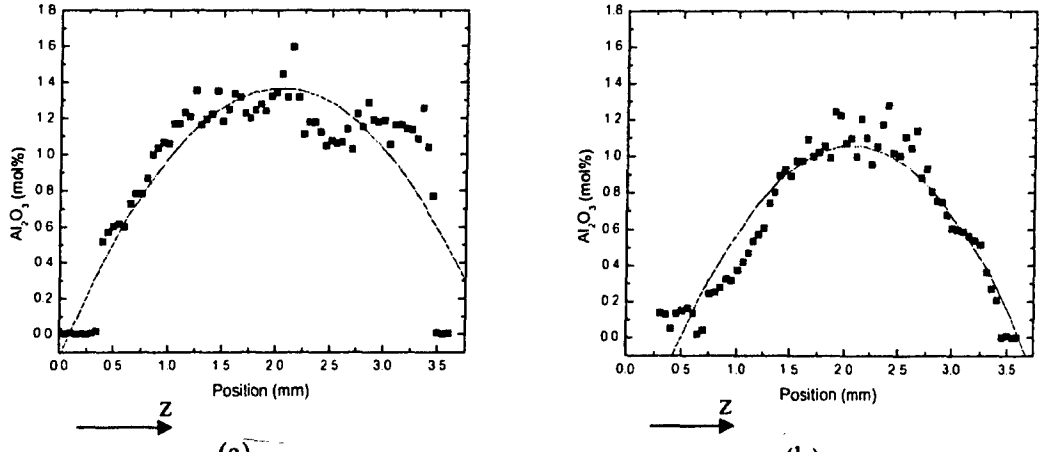

Fig. 8. The dopant distribution of the vertical compositional variation GRIN lenses of (a) Design 2.5% max and (b) Design 1.63% max

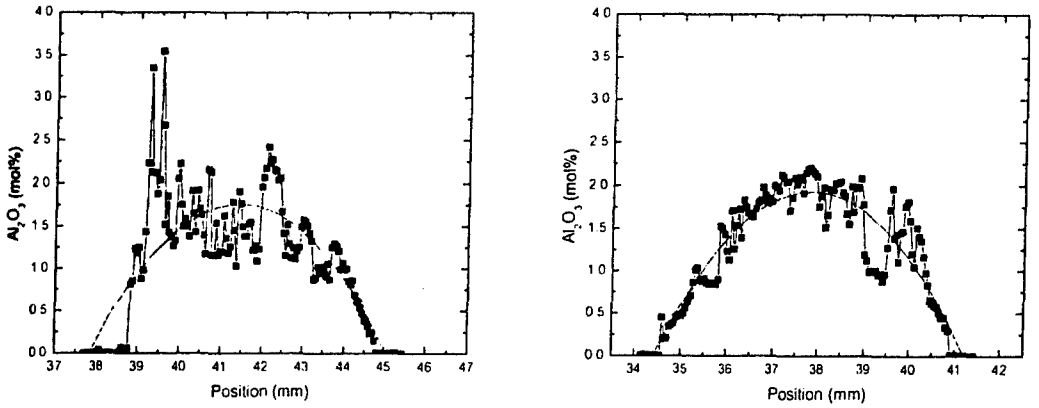

(a) (b)

Fig. 9. The dopant distributions of the GRIN with radial index variation in (a) x-direction and (b) y-direction.

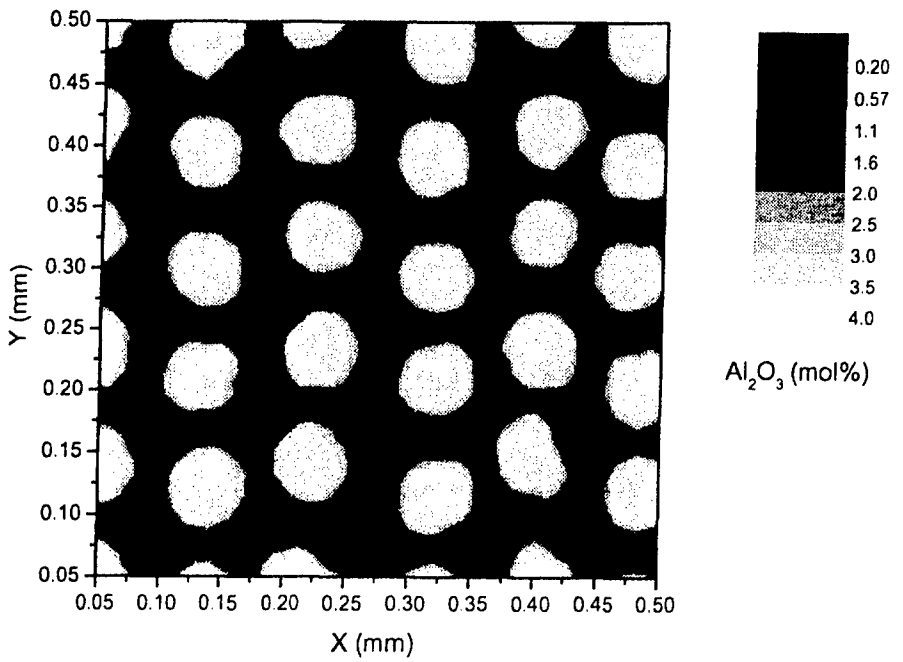

Fig. 10. The 2-dimensional EPMA result of a sintered microlens array.

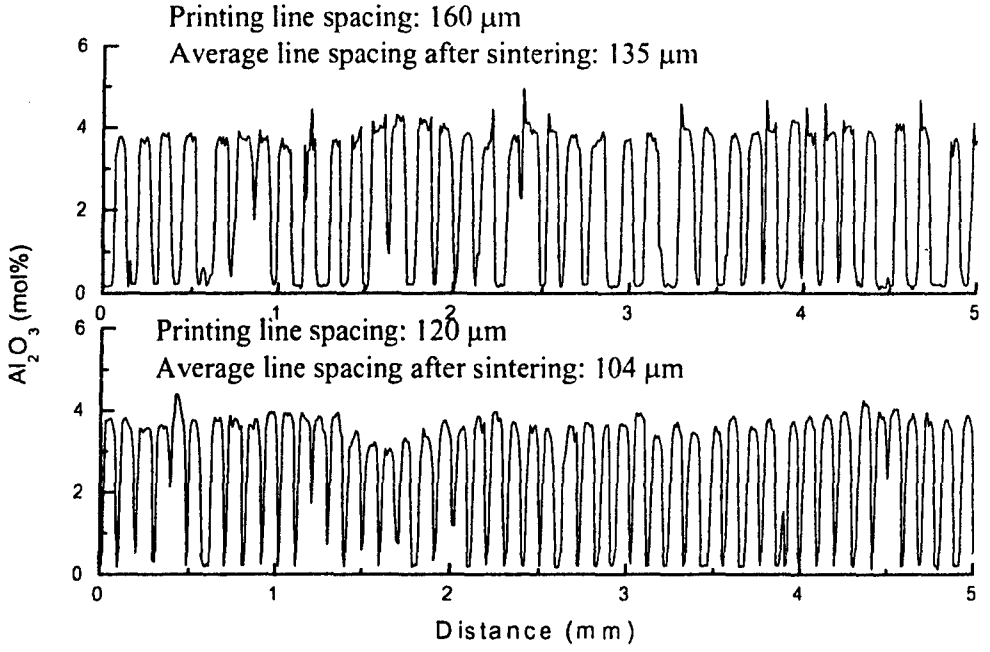

Fig. 11. The EPMA results of the sintered volume phase gratings.

DISCUSSION

The theoretical focal length (f_{th}) of a GRIN slab with a parabolic index of refraction profile is given by the following equation[18]:

$$f_{th} = \frac{1}{\left(\frac{n_{max}^2 - n_{min}^2}{0.25\,w^2}\right)^{1/2} \sin\left(\frac{d}{0.5w}\left(1 - \frac{n_{min}^2}{n_{max}^2}\right)^{1/2}\right)} \quad (2)$$

where w is the width of the GRIN slab, d is the thickness of the GRIN slab, n_{min} is the minimum index of refraction, and n_{max} is the maximum index of refraction. No direct measurement of index of refraction has been made in this study. The index of refraction, n, of fused silicate containing alumina, however, has been found to vary linearly with the alumina content, M, as described by Equation 3[19]:

$$n=1.4580+0.00192M \quad (3)$$

where M is the alumina concentration in mol%. The alumina concentration profiles of the Design 1.63% max and Design 2.5% max samples are shown in Fig. 8. The profiles are fitted with parabolic curves. The maximum alumina concentrations of the Design 1.63% max and Design 2.5% max samples are found to be 1.04 mol% and 1.35 mol% and the maximum indices of refraction (n_{max}) of the samples are calculated to be 1.46 and 1.4606 from Equation (3). The theoretical focal lengths of the sintered powder beds, assuming a parabolic index profile, are then calculated and compared with the effective focal lengths, as shown in Table II. The effective focal length is close to the theoretical value for the Design 1.63% max sample. The relatively larger difference between the effective and theoretical value of the Design 2.5% max sample is due to the fact that the concentration profile is not ideally parabolic. The alumina concentration

profiles of the sintered powder bed with radial compositional variation in x-direction and y-direction, shown in Fig. 9, are also fitted with parabolic curves. The maximum alumina concentrations in x-direction and y-direction on the parabolic curves are found to have values about 1.70 mol% and 1.92 mol%, respectively. The theoretical focal lengths of the radial GRIN lens in x-direction and y-direction can also be calculated by replacing the width (w) of the GRIN slab with the diameter of the radial GRIN lens in Equation 2. The theoretical focal lengths are then calculated to be 52.11 cm in x-direction and 50.77 cm in y-direction from Equation 2, as also shown in Table II. The effective focal length in x-direction (63.75 cm) has about 13 cm difference comparing with the value of the theoretical focal length in x-direction (50.77 cm) calculated previously. The difference can be attributed to the deviation of the concentration profile in x-direction from a parabolic curve, as shown in Fig. 9. The effective focal length in y-direction, however, is close to the value of the effective focal length (52.50 cm) due to the fact that the concentration profile in y-direction is fitted well to the parabolic curve.

Table II. The effective (f_{eff}) and theoretical (f_{th}) focal lengths of different GRIN lenses

	Thickness, d (cm)	*Width(diameter), w* (cm)	f_{eff}(cm)	f_{th} (cm)
Design 1.63% max	0.55	0.30	10.00	10.30
Design 2.5% max	0.60	0.30	6.10	7.28
Radial GRIN lens, x-direction	0.27	0.60	63.75	52.11
Radial GRIN lens, y-direction	0.27	0.63	52.50	50.77

It is noted that the length scale of the concentration deviation in both vertical and radial compositional GRIN lenses is in the scale of millimeters, as shown in Fig. 8 and Fig. 9. Davis and Pask studied the diffusion in the alumina-silica system. Their result showed that the diffusivity of alumina in silica at 1650 °C is between 2×10^{-11} cm^2/s (2.44 mol% Al_2O_3) to 1×10^{-10} cm^2/s (5.35 mol% Al_2O_3)[20]. It is thus unlikely that the deviation is caused by the diffusion of aluminum during sintering at 1650 °C for 30 minutes. Migration of aluminum nitrate solution during the printing process is believed to cause the concentration deviation. Differential slip casting, which occurred during the printing process, is resulted from the different slip casting rates of the powder bed at different positions. The presence of dried dopant within the pore space lowers the slip casting rate and slurry can migrate from slow casting regions to fast casting regions. The slow casting region can have a higher green density than the fast casting region. The capillary force difference between pores then causes the as-deposited aluminum nitrate solution to migrate within the powder bed. This results in the concentration deviation in the concentration variation plane. The asymmetric concentration profile in x-direction of the radial GRIN lens, as shown in Fig. 9(a), is believed to be resulted from the differential slip casting caused by the asymmetric deposition of slurry. The direction of slurry deposition is along x-direction and is symmetric in y-direction. This problem could be solved by alternating the direction of slurry deposition every layer. More experiments will be done to understand and solve the problem in the future.

The theoretical focal length of each microlens can be estimated using Equation 2 and the chemical analysis result from Fig. 10. The maximum alumina concentration is about 3.5 mol% from Fig. 10 and results an index of refraction of 1.4647 from Equation 3. The lens diameter is

77 μm as mentioned previously. The lens thickness is 40 μm since only one layer of microlens array pattern was printed. The theoretical focal length can then be calculated to be 0.28 cm. Shorter focal length can be achieved by increasing the number of printed layers of microlens array pattern. The theoretical focal length is calculated to be 276 μm for a micronlens with the same alumina concentration and lens diameter but with lens thickness of 600 μm. The focal length of each microlens in a micrlens array can be changed as desired since the lens thickness of each microlens can be controlled individually by S-3DP™.

A He-Ne laser source with wavelength of 633 nm was shined perpendicularly to the gratings. Diffraction patterns were observed at a distance of 2.8 m from the gratings. The average dot-to-dot distance in the diffraction pattern of the grating with 135 μm line spacing is 1.44 cm while the average dot-to-dot distance in the diffraction pattern of the grating with 104 μm line spacing is 1.80 cm, as shown in Fig. 12. The results are consistent with the fact that the dot-to-dot distance in the diffraction pattern of a phase grating is inversely proportional to its line spacing when the laser wavelength and observing distance are the same[21].

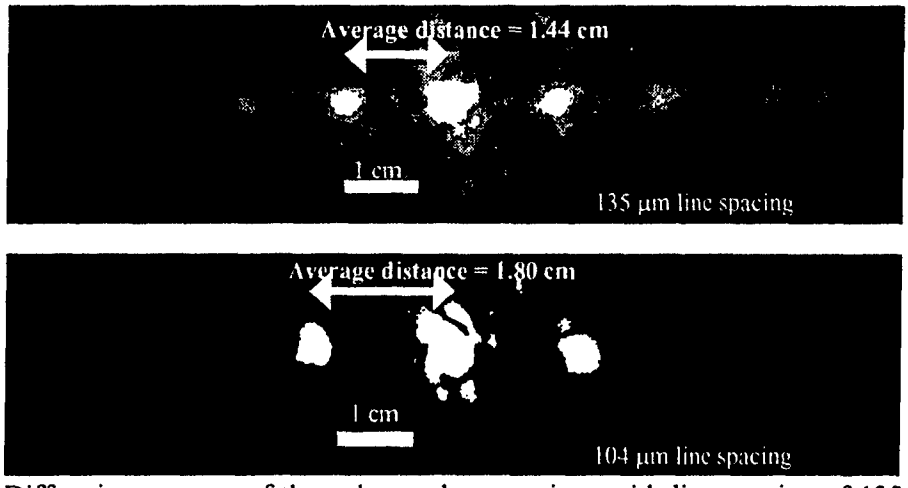

Fig. 12. Diffraction patterns of the volume phase gratings with line spacing of 135 μm and 104 μm, respectively.

CONCLUSION

The alumina-silica system has been studied for the fabrication of GRIN lenses by S-3DP™. Optically transparent alumina-silica GRIN lenses were obtained by sintering at 1650 °C for 30 minutes. GRIN lenses with vertical and radial compositional variations have been successfully fabricated. EPMA results show the deviation of the actual dopant concentration from the designed value. It is believed to be resulted from the different slip casting rates between the doped and un-doped regions in the powder beds. A microlens lens array with a theoretical focal length of 0.28 cm is fabricated as well as the volume phase gratings with line spacing of 104 μm and 135 μm, respectively.

ACKNOWLEDGEMENT

The authors would like to thank Christopher C. Stratton for his help with 3DP™ file generation.

REFERENCES

[1]J. H. Simmons and *et al.*, "Optical Porperties of Waveguides Made by Porous Glass Process," *Applied Optics*, **18** [16] 2732-2733 (1979).

[2]I. Kitano and *et al.*, "A Light Focusing Fiber Guide Prepared by Ion-exchange Techniques," *J. Japan Soc. App. Phys.*, **39**, 63-70 (1970).

[3]J. E. Samuels and D.T. Moore, "Gradient-index Profile Control from Molten Salt Baths," *Applied Optics*, **29** [28] 4042-4050 (1990).

[4]S. Ohmi and *et al.*, "Gradient-index Rod Lens Made by a Double Ion-exchange Process," *Applied Optics*, **27** [3] 496-499 (1988).

[5]S. N. Houde-Walter and D.T. Moore, "Delta-n Control in GRIN glass by Additives in AgCl Diffusion Baths," *Applied Optics*, **25** [19] 3373-3378 (1986).

[6]A. R. Cooper and M.A. el-Leil, "Index Variation from Field-assisted Ion Exchange," *Applied Optics*, **19** [7] 1087-1091 (1980).

[7]A. D. Pearson, W.G. French, and E.G. Rawson, "Perparation of a Light Focusing Glass Rod by Ion-exchange Techniques," *Applied Physics Letters*, **15** [2] 76-77 (1969).

[8]M. Yamane and *et al.*, "Graded Index Materials by the Sol-gel Process," SPIE Optical Engineering Press , 1993.

[9]T. M. Che, J.B. Caldwell, and R.M. Mininni, "Sol-gel Derived Gradient Index Opitcal Materials," *Sol-Gel Optics*, **1328,** 145-159 (1990).

[10]D. T. Moore, "Gradient-Index Optics: A Review," *Applied Optics*, **19** [7] 1035-1038 (1980).

[11] J. M. Tedesco, H. Owen, D. M. Pallister, and M. D. Morris "Principles and Spectroscopic Applications of Volume Holographic Optics", *Analytical Chemistry*, **65** (1993), 441A.

[12]G. Barbastathis and M. Balberg, "Confocal Microscopy with a Volume Holographic Filter", *Optics Letters*, **24** (1999), 811.

[13]E. M. Sachs, M. J. Cima, P. Williams, D. Brancazio and J. Cornie, *J. Eng. Ind.*, **114** (1992) 481.

[14]J. E. Grau, J. Moon, S. Uhland, M. J. Cima and E. M. Sachs, pp. 317-79 in Proceedings of the Solid Freeform Fabrication Symposium, edited by J. J. Beaman, H. L. Marcus, D. L. Bourell, J. W. Barlow and T. Crawford, University of Texas, Austin, TX, 1997.

[15]M. J. Cima, M. Oliveria, H.-R. Wang, E. M. Sachs, and R. Holman, pp. 216-23 in Proceedings of the Solid Freeform Fabrication Symposium, edited by J. J. Beaman, H. L. Marcus, D. L. Bourell, J. W. Barlow and T. Crawford, University of Texas, Austin, TX, 2001.

[16]J. F. MacDowell and G. H. Beall, "Immiscibility and Crystallization in Al_2O_3-SiO_2 Glasses," *J. Am. Ceram. Soc.*, **52** [1] 17-25 (1969).

[17]E. Hecht, "Optics", 4th edition, Addison-Wesley, 2002, p. 159.

[18]B. E. A. Saleh and M. C. Teich, "Fundamentals of Photonics", John Wiley & Sons Inc., New York, 1991, p. 23.

[19]K. Nassau, J. W. Shiever, and J. T. Krause, "Preparation and Properties of Fused Silica Containing Alumina," *J. Am. Ceram. Soc.*, **58** [9-10] 461 (1975).

[20]R. F. Davis and J. A. Pask, *J. Am. Ceram. Soc.*, **55** (1972) 525.

[21]J. W. Goodman, "Introduction to Fourier Optics", 2nd edition, McGraw-Hill, 1996, p.81-83.

APPENDIX B

J. Non-Crystalline Solids 2/27/04 revised

Alumina-doped Silica Gradient-Index (GRIN) Lenses by Slurry-based Three Dimensional Printing (S-3DP^{TM})

Hong-Ren Wang[a], Michael J. Cima[a], Brian D. Kernan[b] and Emanuel M. Sachs[b]

[a] *Department of Materials Science and Engineering, Massachusetts Institute of Technology, Cambridge, MA 02139, USA*
[b] *Department of Mechanical Engineering, Massachusetts Institute of Technology, Cambridge, MA 02139, USA*

Abstract

The traditional slurry-based three-dimensional printing (S-3DP^{TM}) process has been used to fabricate complex structure materials by printing organic binders in selective positions of each printing layer. This process has been modified to fabricate functional graded materials, such as gradient index (GRIN) lenses, by depositing different concentrations of dopant into selective positions. Aluminum nitrate, which decomposes into alumina during heat treatment, is dissolved in deionized water and inkjet printed into the silica powder bed as the source of dopant. Continuous dopant jets and Drop-on-Demand (DoD) printing heads are used to control the dopant concentration profile in one dimension and two dimension, respectively. GRIN lenses with different concentration profiles are fabricated. The alumina-doped silica powder beds are then dehydrated at 1000 °C for 24 hours and sintered to optical transparency at 1650 °C for 30 minutes in a vacuum furnace ($5x10^{-6}$ torr). The dopant distributions after sintering are measured and compared with the design profiles. The resulting optical effects are examined by measuring the effective focal lengths of the GRIN lenses.

Keywords: gradient-index lens, GRIN lens, silica glass, 3DP, three-dimensional printing, functionally graded material.

PACS code: 61.43.Fs, 81.40.Tv.

1. Introduction

Conventional glass-based GRIN lenses, as shown in Fig. 1, have been fabricated by various methods, including molecular stuffing [1], ion exchange [2-7] and sol-gel [8,9] techniques, which rely on stuffing of base glass compositions with index altering cations. The diffusion-controlled nature of these processes results in long processing times (typically > 100 hours), thereby limiting feasible component sizes to less than 13 mm. A comparison of the lens diameter and the index gradient difference (Δn) of radial GRIN rods prepared by various methods is provided in Fig. 1 [8]. The maximum index gradient difference currently produced, i.e., $\Delta n < 0.2$, is limited not only by the base glass composition, but the dopant concentration profiles achievable by these methods. Commercially available SELFOC® lenses, for example, prepared by ion exchange exhibit a maximum Δn value of 0.124 for components ranging in size from 1.0 to 4.5 mm [10]. GRIN materials fabricated by ion exchange techniques are also not suitable for high temperature applications because the migration of alkali ions results in the distortion of the index profile [8]. Alternative materials systems or fabrication methods for large-scale GRIN components with desired optical characteristics and good environmental and thermal stability are needed.

The S-3DP™ technology [11-13] is an agile, facile method of producing near-net shape advanced ceramic components. Parts are constructed in a layer-by-layer build sequence. Each powder bed layer is created by jetting a ceramic slurry onto a substrate. The as-cast layer is then dried and a binder, which cements the ceramic particles, is selectively deposited in the desired pattern. The excess powder is then removed to produce a three dimensional structure. The S-3DP™ process can be modified to fabricate functionally graded materials, such as GRIN lenses, by depositing different amounts of dopant instead of a binder into each layer. The S-3DP™ processes for vertical and radial GRIN lenses are shown schematically in Fig. 2(a) and Fig. 2(b), respectively. Production of GRIN materials by S-3DP™ offers several

advantages over conventional processing methods, including reduced processing times (< 70 hours) yielding economical fabrication of large-scale components, improved compositional flexibility, and increased index profile dimensionality. The improved flexibility and compositional control offered by S-3DP™ results in a single component lens system with greater functionality. The lens stacking required to overcome optical aberrations of a photographic lens system can be eliminated by taking advantages of the additional degree of freedom offered by S-3DP™ GRIN lenses. This research attempts to demonstrate the concept of utilizing S-3DP™ to the fabrication of larger scale GRIN lenses. Several silica-based material systems have been considered. The selecting criteria of the silica-based material system for the fabrication of S-3DP™ GRIN lenses include the ability to change the index of refraction of silica, the existing glass-forming region with silica and the availability of the aqueous salt solution of the dopant. Titania and alumina with their salt solutions of titanium(IV) bis(ammonium lactato) dihydroxide ($[CH_3CH(-O)CO_2NH_4]_2Ti(OH)_2$) and aluminum nitrate ($Al(NO_3)_3*9H_2O$) were selected and tested. It was found that titania-doped silica can be sintered at 1750 ^{0}C but the light scattering due to the crystallization of titania is not suitable for this application. Other material systems, such as bairum-doped silica glass, will be investigated in the future. The alumina-doped silica glass, as a result, was chosen as the material system.

2. Experimental

The amorphous silica powder (Mitsubishi Chemical Company) used in this research had a median particle size of 1.4 μm and a surface area of 2.666 m^2/g. Aluminum nitrate nanohydrate ($Al(NO_3)_3*9H_2O$, Alfa Aesar) was used as the dopant source. Vertical index variation GRIN lenses were fabricated from a 30 vol% silica slurry, while a 22.5 vol% slurry was used to fabricate the radial index variation GRIN lens. Both slurries were ball-milled

with glass media for 20 hours before printing. The chemical compositions of the slurries are shown in Table 1. Boric Acid was added to lower the sintering temperature.

Aluminum nitrate-doped silica powder beds with vertical compositional variation were fabricated by S-3DP™ using a continuous dopant jet. The vertical compositional variation was achieved by printing different concentrations of aluminum nitrate solution while keeping the flow rate of the continuous dopant jet unchanged. The thickness of each printed layer was 73 μm. Two vertical concentration profiles with maximum concentration in the center were printed to create two vertical GRIN lenses with different optical effects, shown in Fig. 3. Each printed slurry layer and dopant layer was dried at 65 ^{0}C for 50 seconds and 55 layers were printed. Aluminum nitrate-doped silica powder beds with radial compositional variation were made with a 3DP™ machine equipped with Drop-on-Demand (DoD) printing nozzles, which allow the dopant solution to be deposited in selective region drop by drop. The drop size of the aluminum nitrate solution was 45 μm. The thickness of each dried slurry layer was 40 μm. The designed concentration profile is shown in Fig. 4. Each printed slurry layer was dried at 100 ^{0}C for 50 seconds while each printed dopant layer was dried in a microwave oven for 1 minute.

The aluminum nitrate-doped silica powder beds were heated at a temperature of 900°C for 4 hours in air to remove the hydroxyl groups introduced by the aluminum nitrate solution as well as the organic additives. Sintering was performed in a vacuum furnace (Centoor, MRF, pressure ~ $5x10^{-6}$ torr) at various temperatures, holding times, and cooling rates. It was found that un-doped silica powder beds were sintered into optical transparency at 1500°C for 30 minutes, as shown in Fig. 5. An additional dehydration process at 1000 ^{0}C for 24 hours in the vacuum furnace for powder beds with a maximum alumina concentration of 2.50 mol% was required to completely remove the residual hydroxyl groups that form bubbles during sintering.

X-ray Diffraction (XRD) was used to detect crystallization of the doped powder bed after heat treatment. The sintered powder beds were polished and observed under an optical microscope. Chemical compositions of the doped powder beds were measured by electron probe microanalysis (EPMA, JOEL Superprobe 733).

3. Results

The mixture of alumina and silica tends to form mullite ($3Al_2O_3+2SiO_2$) at temperature higher than 950 °C [14]. The formation of mullite can be minimized by increasing the cooling rate and using the alumina concentration lower than 5 mol% [14]. The maximum alumina concentration in this study was 2.50 mol% (Fig. 4). XRD result shows no crystallization in the alumina-silica powder beds that were treated at 900 °C for 4 hours, as shown in Fig. 6. Several sintering conditions were tested. Optical transparency was achieved for the alumina-doped powder beds by sintering at 1650 °C for 30 minutes and cooling at the maximum rate (~500 ^{0}C/minute from the sintering temperature) allowed by the furnace. Two alumina-doped powder beds with vertical compositional variation were sintered. The designed maximum concentrations of these two samples are 1.63 mol% (Design 1.63% max) and 2.50 mol% (Design 2.50% max), as shown in Fig. 3. The alumina-doped powder bed with radial compositional variation was also sintered using the same sintering condition.

The magnifying effects of the sintered powder beds with vertical compositional variation are shown in Fig. 7. The MIT markers under the sintered powder beds are magnified in the vertical direction, as expected from the dopant concentration profile shown in Fig. 3. The object and image sizes in the vertical direction were measured, allowing the effective focal length (f_{eff}) to be determined by the following equation [15]:

$$\frac{1}{f_{\text{eff}}} = \frac{1}{S_1} - \frac{H_1}{H_2 * S_1} \qquad (1)$$

where H_1 is the object size, H_2 is the image size, and S_1 is the distance between the lens and the object. The effective focal lengths of the powder beds with vertical compositional variation were calculated to be 10 cm and 6.1 cm for Design 1.63% max and Design 2.50 max, respectively. The magnifying effect of the sintered powder bed with radial compositional variation is shown in Fig. 8. The effective focal lengths were also calculated to be 63.75 cm in x-direction and 52.50 cm in y-direction using the same method. The chemical composition profiles of the sintered powder beds with vertical compositional variation measured by EPMA are shown in Fig. 9 while the chemical composition profiles in x-direction and y-direction of the sintered powder bed with radial compositional variation are shown in Fig. 10. It is noted that the measured concentration profiles deviate from the designed concentration profiles, as shown in Fig. 3 and Fig. 4.

4. Discussion

The theoretical focal length (f_{th}) of a GRIN slab with a parabolic index of refraction profile is given by the following equation [16]:

$$f_{th} = \frac{1}{\left(\frac{n_{max}^2 - n_{min}^2}{0.25\,w^2}\right)^{1/2} \sin\left(\frac{d}{0.5w}\left(1 - \frac{n_{min}^2}{n_{max}^2}\right)^{1/2}\right)} \quad (2)$$

where w is the width of the GRIN slab, d is the thickness of the GRIN slab, n_{min} is the minimum index of refraction, and n_{max} is the maximum index of refraction. No direct measurement of index of refraction has been made in this study. The index of refraction, n, of fused silicate containing alumina, however, has been found to vary linearly with the alumina content, M, as described by Equation 3 [17]:

$$n=1.4580+0.00192M \quad (3)$$

where M is the alumina concentration in mol%. The alumina concentration profiles of the Design 1.63% max and Design 2.5% max samples are shown in Fig. 9. The profiles are fitted with parabolic curves. The maximum alumina concentrations of the Design 1.63% max and Design 2.5% max samples are found to be 1.04 mol% and 1.35 mol% and the maximum indices of refraction (n_{max}) of the samples are calculated to be 1.46 and 1.4606 from Equation (3). The theoretical focal lengths of the sintered powder beds, assuming a parabolic index profile, are then calculated and compared with the effective focal lengths, as shown in Table 2. The effective focal length is close to the theoretical value for the Design 1.63% max sample. The relatively larger difference between the effective and theoretical value of the Design 2.5% max sample is due to the fact that the concentration profile is not ideally parabolic. The alumina concentration profiles of the sintered powder bed with radial compositional variation in x-direction and y-direction, shown in Fig. 10, are also fitted with parabolic curves. The maximum alumina concentrations in x-direction and y-direction on the parabolic curves are found to have values about 1.70 mol% and 1.92 mol%, respectively. The theoretical focal lengths of the radial GRIN lens in x-direction and y-direction can also be calculated by replacing the width (w) of the GRIN slab with the diameter of the radial GRIN lens in Equation 2. The theoretical focal lengths are then calculated to be 52.11 cm in x-direction and 50.77 cm in y-direction from Equation 2, as also shown in Table 2. The effective focal length in x-direction (63.75 cm) has about 13 cm difference comparing with the value of the theoretical focal length in x-direction (50.77 cm) calculated previously. The difference can be attributed to the deviation of the concentration profile in x-direction from a parabolic curve, as shown in Fig. 10. The effective focal length in y-direction, however, is close to the value of the effective focal length (52.50 cm) due to the fact that the concentration profile in y-direction is fitted well to the parabolic curve. The relatively long focal length of the GRIN lenses by S-3DP^{TM} compared to the commercially available GRIN

lenses is due the fact that the ability of alumina to change the index of refraction of silica is small. It is known from Equation 2 that the focal length of a GRIN lens becomes shorter when the thickness (d) of the GRIN lens becomes thicker. The required thickness is calculated from Equation 2 to be 2.97 cm in order to make a GRIN lens with a maximum alumina concentration of 1.7 mol%, a focal length of 5 cm and a diameter of 0.60 cm. It requires about 800 of 3DP^{TM} layers to have a final thickness of 2.97 cm after sintering. The total processing time is thus increased. The required thickness for a GRIN lens with the same maximum alumina concentration and focal length but a diameter of 0.2 cm is also calculated to be 0.31 cm, which requires about 86 of 3DP^{TM} layers. Dopants with higher ability to change the index of refraction of silica, such as barium oxide, will be investigated in the future.

It is noted that the length scale of the concentration deviation in both vertical and radial compositional GRIN lenses is in the scale of millimeters. Davis and Pask studied the diffusion in the alumina-silica system. Their result showed that the diffusivity of alumina in silica at 1650 °C is between 2×10^{-11} cm^2/s (2.44 mol% Al_2O_3) to 1×10^{-10} cm^2/s (5.35 mol% Al_2O_3) [18]. It is thus unlikely that the deviation is caused by the diffusion of aluminum during sintering at 1650 °C for 30 minutes. Migration of aluminum nitrate solution during the printing process is believed to cause the concentration deviation. Differential slip casting, which occurred during the printing process, is resulted from the different slip casting rates of the powder bed at different positions. The presence of dried dopant within the pore space lowers the slip casting rate and slurry can migrate from slow casting regions to fast casting regions. The slow casting region can have a higher green density than the fast casting region. The capillary force difference between pores then causes the as-deposited aluminum nitrate solution to migrate within the powder bed. This results in the concentration deviation in the concentration variation plane.

Further observation of the samples with vertical compositional variation using optical microscope shows a layered structure perpendicular to the built direction, as shown in Fig. 11. Light diffraction was also seen, as shown in Fig. 12, when a laser was shined through the sample normally to the plane of concentration variation. Fig. 11 and Fig. 12 indicate locally inhomogeneous distribution of dopant in each printed layer. Fig. 13 shows the alumina concentrations along z-direction in the sample with radial compositional variation. Locally compositional variation with an average peak-to-peak distance of about 36 μm is observed in Fig. 13. The length scale of the compositional variation is close to the green slurry layer thickness of 40 μm. It is therefore believed that the migration of dopant solution also happens during the drying of each printed layer. Similar phenomenon, segregation of chemical additives during drying, was also observed in the tape casting process [19]. The additives are carried with the solvent flowing toward the top of the drying surface and accumulated on the top of the drying surface after the solvent evaporates. Locally inhomogeneous distribution of additives along z-direction within each printed layer is thus created.

5. Conclusion

The alumina-silica system has been studied for the fabrication of GRIN lenses by S-3DP™. Optically transparent alumina-silica GRIN lenses were obtained by sintering at 1650 °C for 30 minutes. GRIN lenses with vertical and radial compositional variations have been successfully fabricated. EPMA results show the deviation of the actual dopant concentration from the designed value. Migration of dopant during printing and segregation of dopant during drying are the main causes of concentration deviation. Further research will focus on more precise local composition control both in the concentration variation plane and in z-direction.

Acknowledgement

This research was supported by United States Army Research Office under grant number DAAD19-00-1-0124. The authors would like to thank Christopher C. Stratton for his help with 3DP™ file generation.

References

[1] J. H. Simmons and *et al.*, Appl. Opt., 18 (1979) 2732.

[2] I. Kitano and *et al.*, J. Japanese Soc. Appl. Phys., 39 (1970) 63.

[3] J. E. Samuels and D. T. Moor, Appl. Opt., 29 (1990) 4042.

[4] S. Ohmi and *et al.*, Appl. Opt., 27 (198) 496.

[5] S. N. Houde-Walter and D.T. Moore, Appl. Opt., 25 (1986) 3373.

[6] A. R. Cooper and M.A. el-Leil, Appl. Opt., 19 (1980) 1087.

[7] A. D. Pearson, W.G. French, and E.G. Rawson, Appl. Phys. Lett., 15 (1969) 76.

[8] M. Yamane and *et al.*, "Graded Index Materials by the Sol-gel Process," SPIE Optical Engineering Press , 1993.

[9] T. M. Che, J.B. Caldwell, and R.M. Mininni, Sol-Gel Optics, 1328 (1990) 145.

[10] D. T. Moore, Appl. Opt., 19 (1980) 1035.

[11] E. M. Sachs, M. J. Cima, P. Williams, D. Brancazio and J. Cornie, J. Eng. Ind., 114 (1992) 481.

[12] J. E. Grau, J. Moon, S. Uhland, M. J. Cima and E. M. Sachs, pp. 317-79 in Proceedings of the Solid Freeform Fabrication Symposium, edited by J. J. Beaman, H. L. Marcus, D. L. Bourell, J. W. Barlow and T. Crawford, University of Texas, Austin, TX, 1997.

[13] M. J. Cima, M. Oliveria, H.-R. Wang, E. M. Sachs, and R. Holman, pp. 216-23 in Proceedings of the Solid Freeform Fabrication Symposium, edited by J. J. Beaman, H.

L. Marcus, D. L. Bourell, J. W. Barlow and T. Crawford, University of Texas, Austin, TX, 2001.

[14] J. F. MacDowell and G. H. Beall, J. Am. Ceram. Soc., 52 (1969) 17.

[15] E. Hecht, Optics, 4th edition, Addison-Wesley, 2002, p. 159.

[16] B. E. A. Saleh and M. C. Teich, Fundamentals of Photonics, John Wiley & Sons Inc., New York, 1991, p. 23.

[17] K. Nassau, J. W. Shiever, and J. T. Krause, J. Am. Ceram. Soc., 58 (1975) 461.

[18] R. F. Davis and J. A. Pask, J. Am. Ceram. Soc., 55 (1972) 525.

[19] J.-H. Jean and H.-R. Wang, J. Am. Ceram. Sco., 84 (2001) 267.

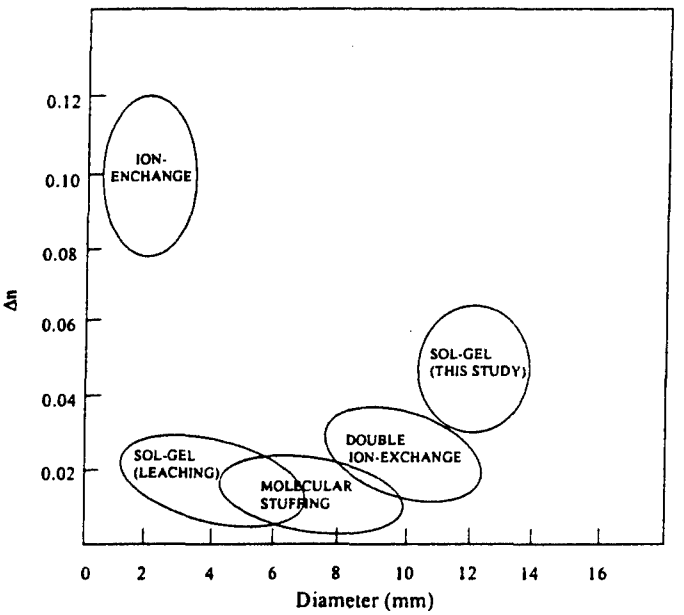

Fig. 1. Comparison of the lens diameter and Δn of radial GRIN rods prepared by various methods.[8]

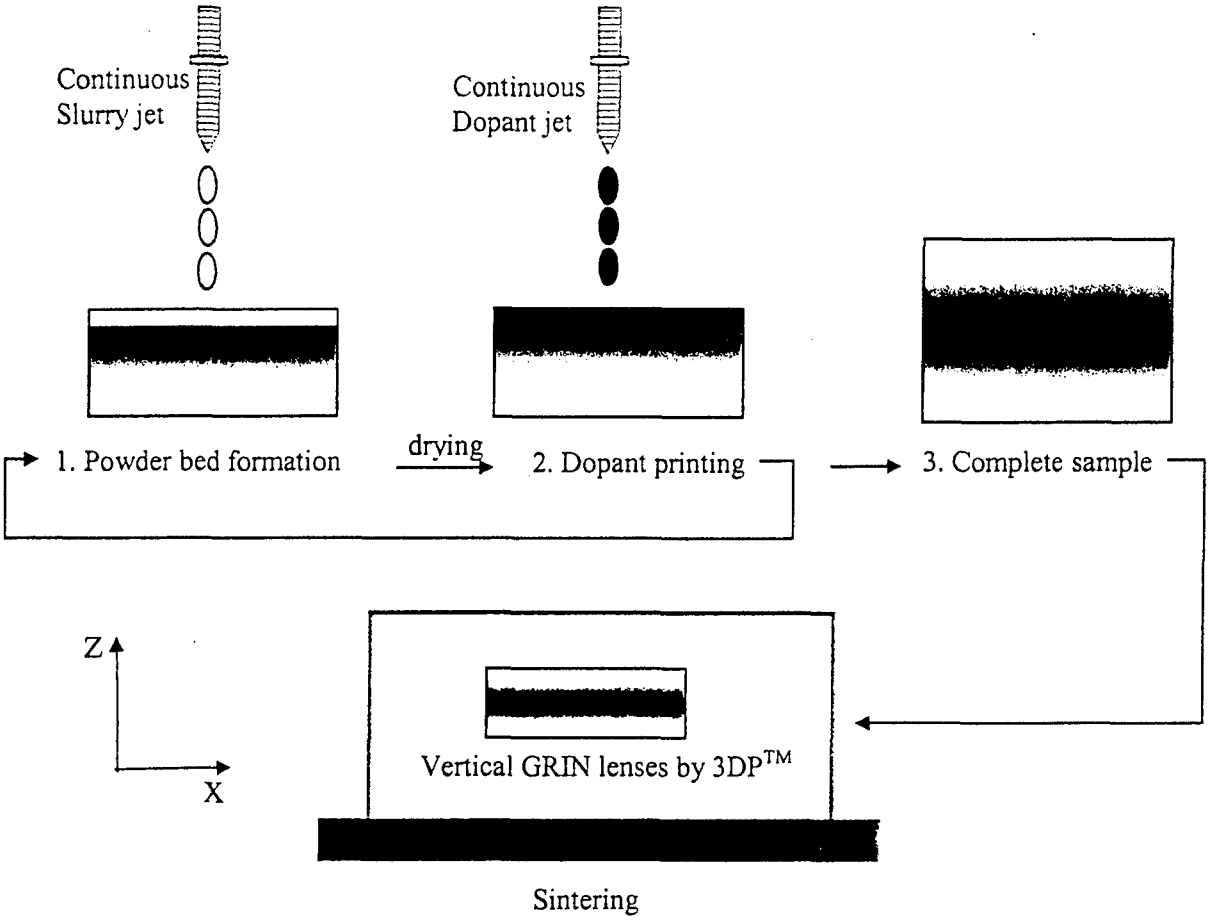

Fig. 2(a). The schematic drawing of the S-3DP™ process for vertical GRIN lenses.

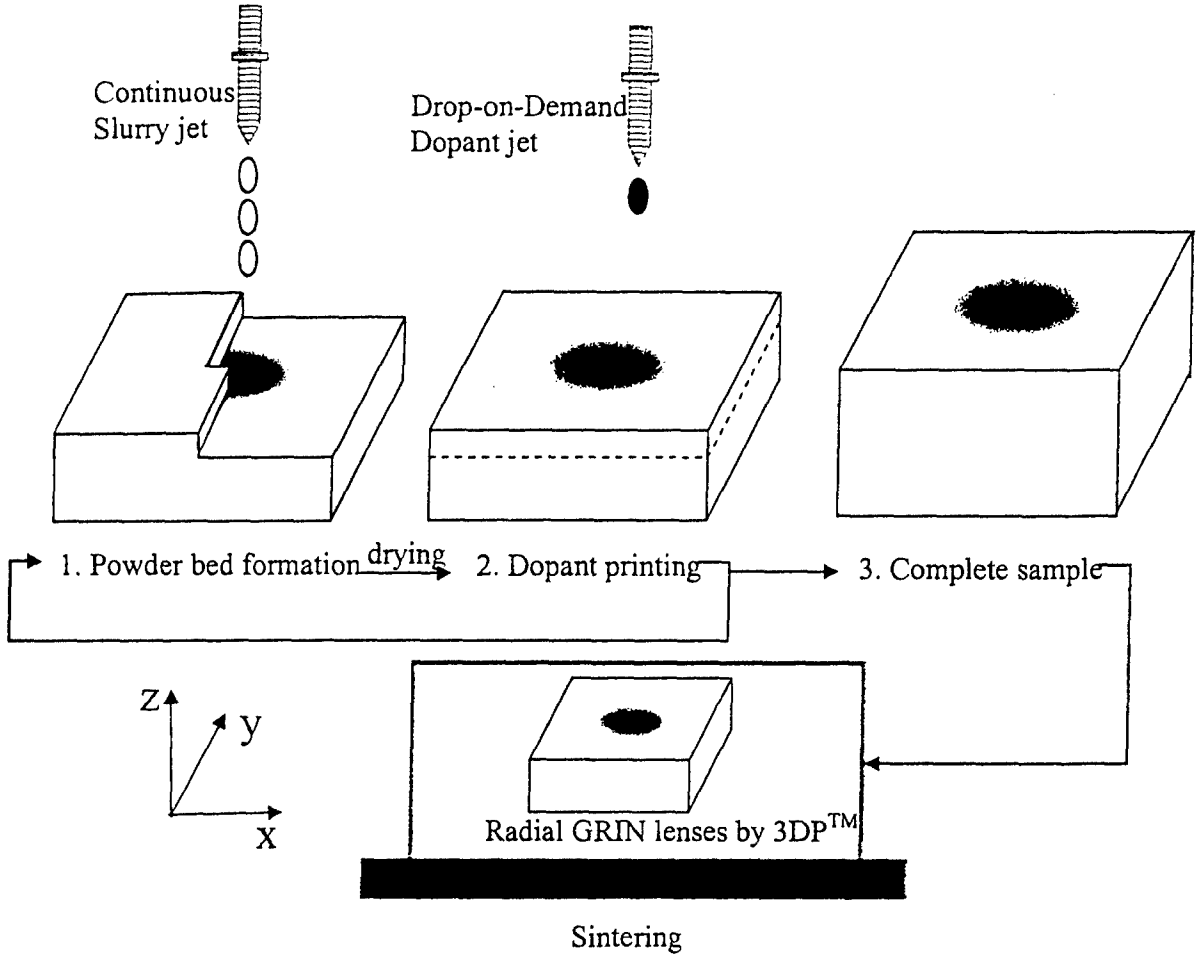

Fig. 2(b). The schematic drawing of the S-3DP™ process for radial GRIN lenses.

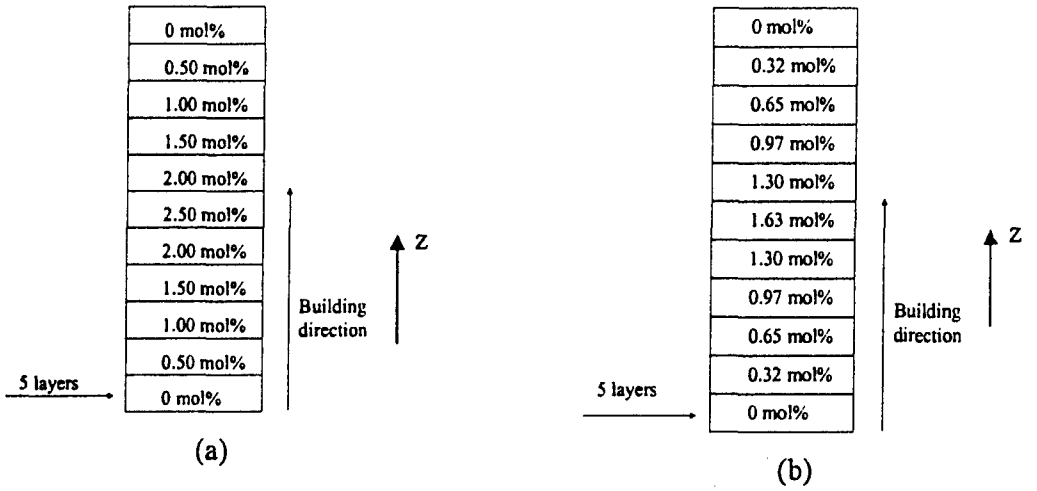

Fig. 3. The concentration profiles of alumina in the GRIN lenses of (a) Design 2.5% max and (b) Design 1.63% max.

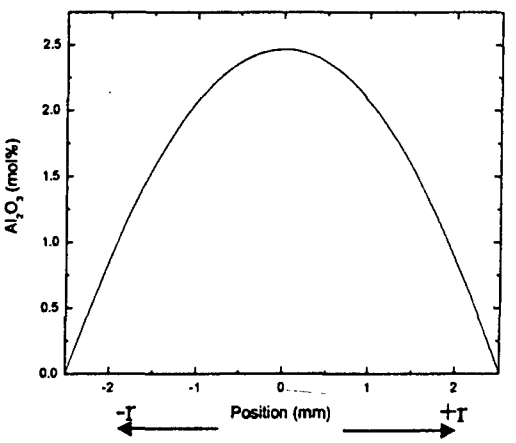

Fig. 4. The concentration profile of the GRIN lens with radial index variation

Table 1
The chemical compositions of the silica slurries.

Silica Powder (vol%)	Deionized Water (vol%)	Methanol (vol%)	2-Propanol (vol%)	Poly (ethylene glycol) (MW:400)	TMAH* (M)	NH_4OH (M)	H_3BO_3 (wt%)
30	35	35	0	3 wt% based on silica	0	0.20	1 wt% based on silica
22.5	38.75	0	38.75	0	0.063	0	1 wt% based on silica

*tetramethylammonium hydroxide

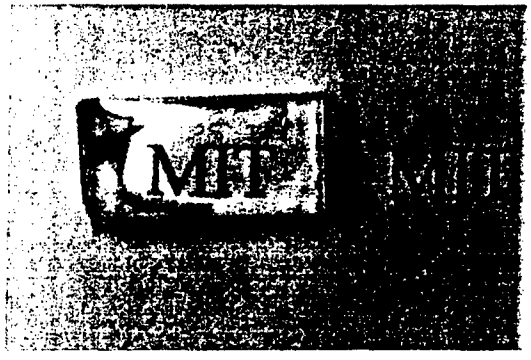

Fig. 5. The transparent un-doped silica powder bed sintered at 1500 °C for 30 minutes.

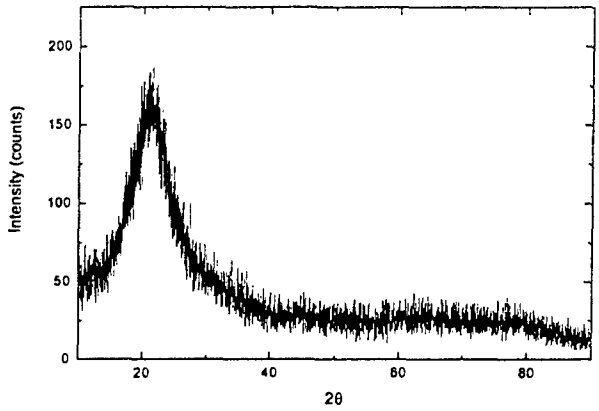

Fig. 6. The XRD result of the alumina-silica powder bed treated at 900 °C for 4 hours.

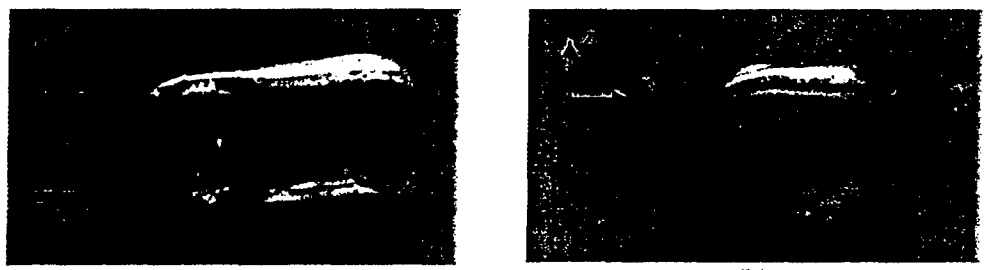

(a) (b)

Fig. 7. The vertical enlargement with the alumina-doped GRIN lenses above an MIT marker. (a)Maximum alumina concentration: 1.63 mol%, (b)Maximum alummina concentration: 2.50 mol%

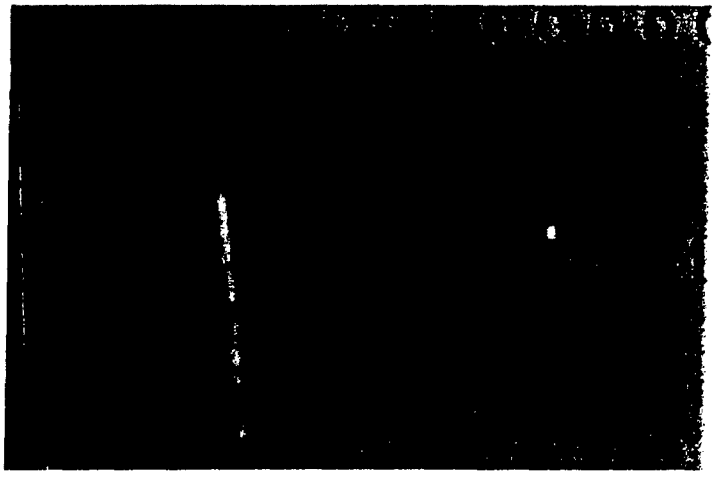

Fig. 8. The enlargement with the radial alumina-doped GRIN lenses.

Table 2

The effective (f_{eff}) and theoretical (f_{th}) focal lengths of different GRIN lenses

	Thickness, d (cm)	*Width(diameter), w* (cm)	f_{eff}(cm)	f_{th} (cm)
Design 1.63% max	0.55	0.30	10.00	10.30
Design 2.5% max	0.60	0.30	6.10	7.28
Radial GRIN lens, x-direction	0.27	0.60	63.75	52.11
Radial GRIN lens, y-direction	0.27	0.63	52.50	50.77

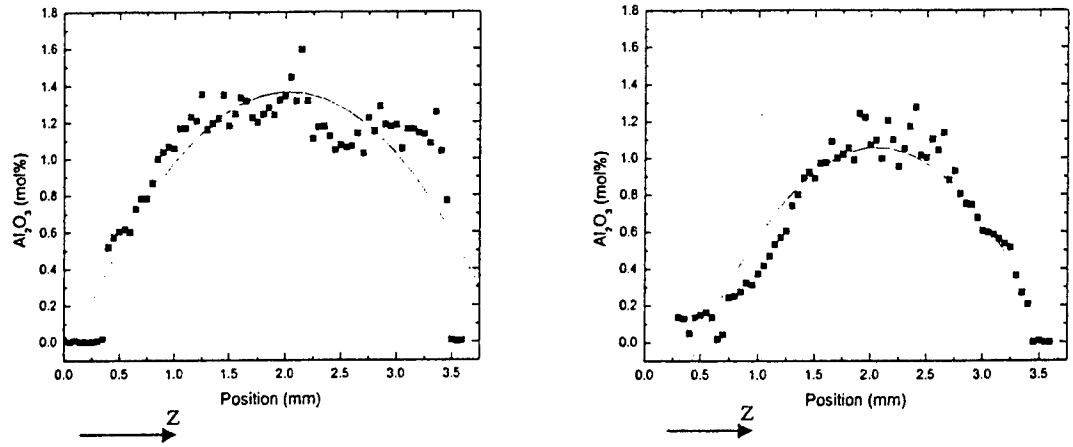

Fig. 9. The dopant distribution of the vertical compositional variation GRIN lenses of (a) Design 2.5% max and (b) Design 1.63% max

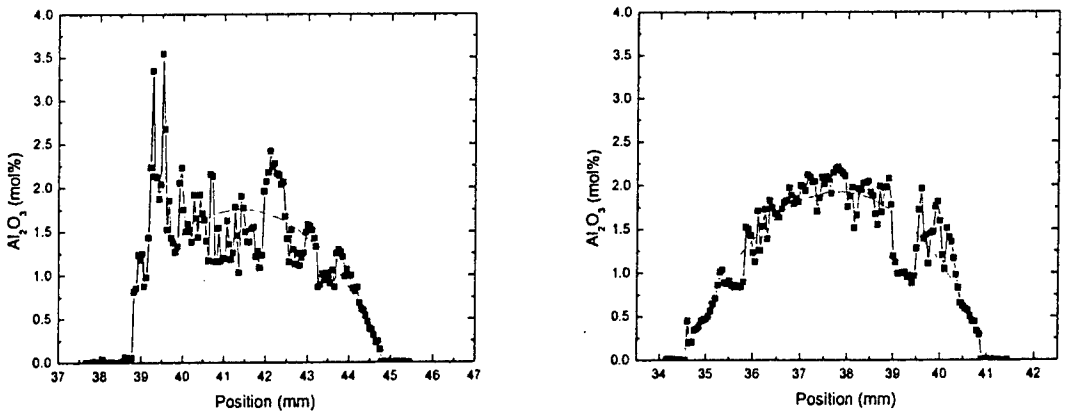

Fig. 10. The dopant distributions of the GRIN with radial index variation in (a) x-direction and (b) y-direction.